A Hydraulic Study of the Exchange Flow through the Burlington Ship Canal

Amina Jalili

A thesis

in

Department

Of

Building, Civil and Environmental Engineering

Presented in Partial Fulfillment of the Requirements
for the Degree of Master of Applied Science (Civil Engineering) at
Concordia University
Montreal, Quebec, Canada

April 2010

Your file Votre référence
ISBN: 978-0-494-67118-4
Our file Notre référence
ISBN: 978-0-494-67118-4

Abstract

A hydraulic study of the exchange flow through the Burlington Ship Canal

Amina Jalili

This thesis is an investigation on the exchange flow through the Burlington Ship Canal, which connects Hamilton Harbour with Lake Ontario. During the summer months, heavily polluted Hamilton Harbour water flows through the canal into the lake, whereas fresh and oxygenated Lake Ontario water flows into the harbour. This exchange of the two water masses has important implications for harbour water quality. This thesis is probably the first modelling investigation of two-layer hydraulic exchange flow, which allows for the effects of both friction and time-dependent barotropic forcing at multiple frequencies. In the Burlington Ship Canal application we obtain predictions of exchange volume fluxes under a range of prevailing forcing conditions that are derived from field observations. Model results compare well with experimental and field data.

Acknowledgements

I would like to sincerely express my gratitude to all those who gave me the possibility to complete this thesis. Especially, I want to thank my supervisor Dr. S. Samuel Li who provided guidance and encouragement necessary to complete this study. I would like to thank the Staff in Department of Building, Civil and Environmental Engineering especially Debbie Walker, for all her encouragement and support. I must acknowledge David Adesina During's help for editing.

In addition, I appreciate all the encouragement I have ever received from my family and friends throughout my academic career. Finally, I thank my mother, who has always encouraged me to pursue higher education.

Table of Contents

List of Figures:

List of Tables:

List of Symbols

A : area of lower layer

a : total cross-sectional area of the channel

a_1 : cross-sectional area at a given location in the channel for upper layer

a_2 : cross-sectional area at a given location in the channel for lower layer

B : Burlington Ship Canal's width

b : model channel width

b^* : dimensionless model channel width

c : phase speed

cm : centimetre

E : East

F_b : bottom force

F_w : wall force

F_{1w} : upper layer wall force

F_{2w} : lower layer wall force

F_{1I} : upper layer interfacial force

F_{2I} : lower layer interfacial force

f_b : bottom friction coefficient

f_w : wall friction coefficient

f_I : interfacial friction coefficient

h :hour

g : gravity

g' : reduced gravity

L : Burlington Ship Canal's length

m : meter

N : North

n : number of wave nodes over the length of the canal

r_i : ratio of interfacial friction coefficient to bottom friction coefficient

r_w : ratio of sidewall friction coefficient multiplied by the total depth of flow to bottom friction coefficient multiplied by the width of channel

s :second

S_b :bottom friction

S_{1i} : interface friction for upper layer

S_{2i} : interface friction for lower layer

S_{1w} : sidewall friction for upper layer

S_{2w} : sidewall friction for lower layer

Q_1 : outflow from the harbour

Q_2 : inflow from the lake

$\overline{Q}$: predicted unsteady volume flux

$\overline{Q}_{12h}$: 12-hour average flow

$\overline{Q}_{15\,\min}$: fifteen-minute average flows

Q_{inv} : theoretical volume flux

Q_{pred} : predicted volume flux

q : volumetric flux

q_o : amplitude of barotropic flux

q^* : dimensionless volumetric flux

q_2^* : time-dependent exchange flux per unit width of canal

$\overline{q}_2^*$: time average of volume fluxes over one or more time periods of barotropic forcing

$\overline{q}_1$: time average of volume fluxes for upper layer

$\overline{q}_2$: time average of volume fluxes for lower layer

q_n : amplitude of the n'th mode barotropic forcing

T : Burlington Ship Canal's time period

T_n : Time period of standing waves of the n'th mode barotropic forcing

t : time

t^* : dimensionless time

u_o : depth-average fluid velocity through the model channel

u_1 :fluid velocity for upper layer

u_2 : fluid velocity for lower layer

u_1^* :dimensionless fluid velocity for upper layer

u_2^* : dimensionless fluid velocity for lower layer

u_b : velocity of barotropic or depth-average flow

V :maximum layer velocity

Vol : Lower layer volume

W : West

x : horizontal coordinates

x^* : dimensionless horizontal coordinates

Y : Burlington Ship Canal's depth

y_1 : upper layer height

y_2 : lower layer height

y_1^* : dimensionless upper layer thickness

y_2^* : dimensionless lower layer thickness

α : measures the relative importance of frictional effects to inertial effects

β : measures the strength of the barotropic flow relative to the velocity scale of the density-driven flow

γ : represents the ratio of the forcing period to the time scale for interface waves to travel through the canal

Δx : lower layer's length along-channel direction

Δu : total of upper and lower layer fluid velocities

Δu^* : dimensionless total of upper and lower layer fluid velocities

θ_n : initial phase of the n'th mode of barotropic forcing

π :pi

ρ_1 : density for upper layer

ρ_2 : density for lower layer

τ_b : bottom frictional drag per unit area

τ_w : sidewall frictional drag per unit area

τ_{1w} : lower layer frictional drag per unit area

τ_{2w} : upper layer frictional drag per unit area

ν :kinematic viscosity

Chapter One: Introduction

1.1 Background

In a channel connecting two water bodies of uniform but slightly different fluid densities, a layered, oppositely flowing exchange of the two fluids often takes place. Different densities between the water bodies may arise from differences in temperature, salinity and/or suspended-sediment concentration. The Burlington Ship Canal connects Hamilton Harbour with Lake Ontario (Figure 1.1). During the summer months, there are water temperature differences between the two ends of the canal, causing exchange flow through the canal (Figure 1.2).

Temperature differences of around 10^{o} C have been observed (Dick and Marsalek, 1973). As a result, an upper layer of warmer water flows out of the harbour into the lake (Figure 1.3), whereas a lower layer of cooler water flows from the lake into the harbour. This exchange of water through the Burlington Ship Canal is the largest component of the water balance around the harbour (Tedford, 1999). It represents the most significant source of fresh, oxygenated water for the harbour from Lake Ontario. The other input sources are mainly tributaries, treated sewage effluents and industrial discharges.

Well-known examples of density-driven exchange flow through man-made channels and natural sea straits include:

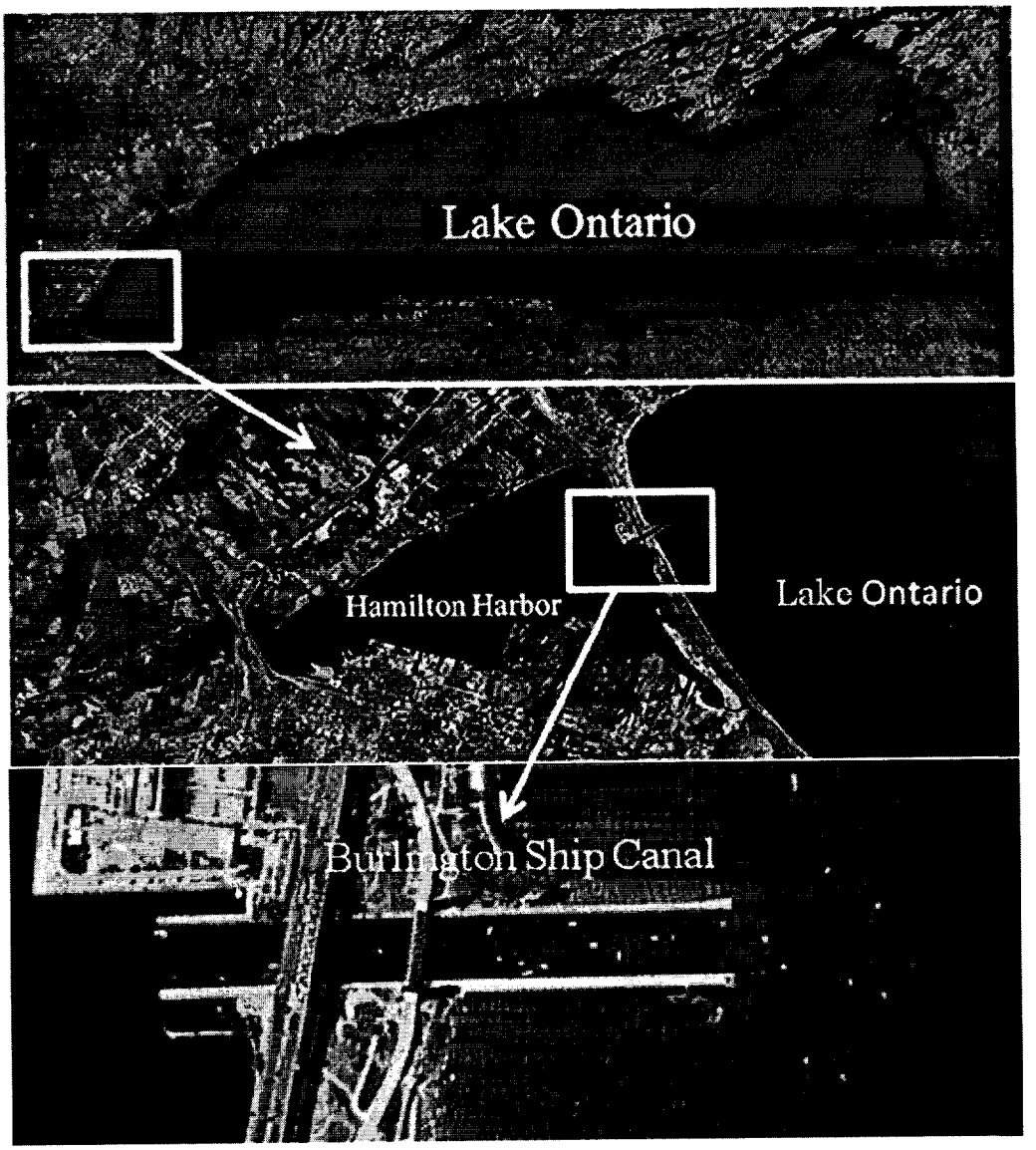

Figure 1.1: Map of the study site, showing Lake Ontario, Hamilton Harbour and the Burlington Ship Canal (from Google Earth, accessed on February 20, 2010). The midpoint of the canal is located at (43°17'57.57" N, 79°47'41.27" W). The canal was built in the 1820s for sailing vessels. Its dimensions are 89 m wide, 10.6 m deep (on average) and 830 m long.

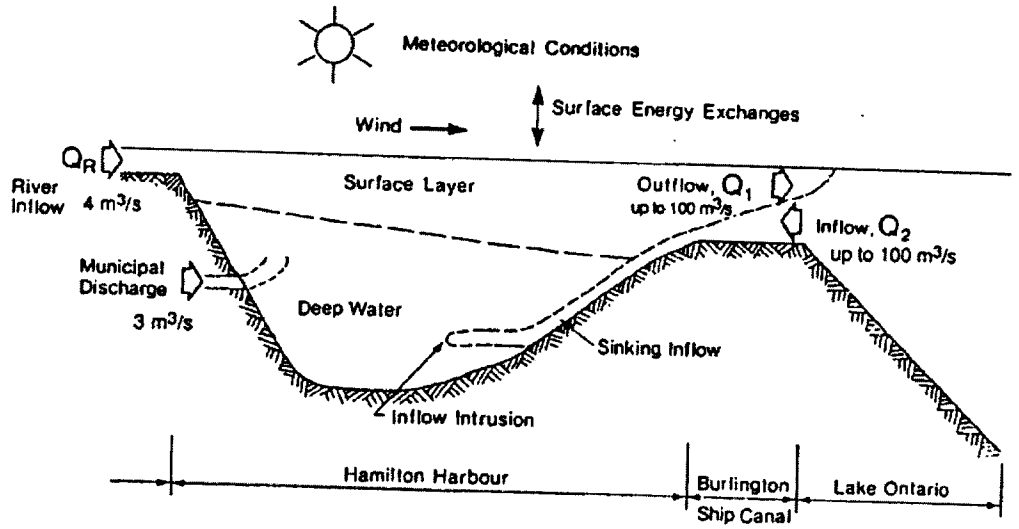

Figure 1.2: Schematic of the exchange flow through the Burlington Ship Canal. Warm, buoyant outflow from the harbour is denoted by Q_1 and cooler, denser inflow from the lake is denoted by Q_2. (Adapted from Hamblin, 1989)

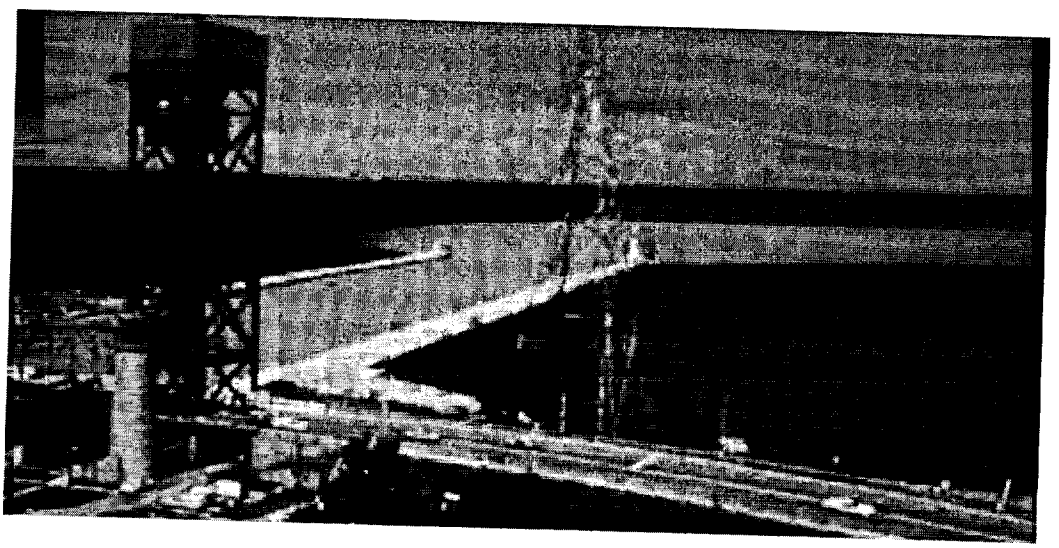

Figure1.3: The eastern section of the Burlington Ship Canal, showing the outflow plume of polluted Harbour Water (brown) into the lake (blue). (Adapted from Lawrence et al., 2004)

- the exchange between the Mediterranean Sea (denser) and Atlantic Ocean through the Strait of Gibraltar (Defant, 1961; Armi and Farmer, 1988),
- the exchange between the Mamara Sea (saltier) and Black Sea through the Bosphorus Strait (Gregg and Ozsoy, 2000), and
- the exchange between the North Sea (saltier) and Baltic Sea through the Great Belt, a strait between the Danish islands of Zealand and Funen (Ottesen-Hansen and Moeller, 1990).

These exchange flows are of oceanographic, geophysical and engineering relevance.

This study of the exchange flow through the Burlington Ship Canal has been motivated by its relevance to important water quality issues facing Hamilton Harbour. The harbour has been receiving a large amount of industrial and domestic waste effluents. They have contributed to poor water clarity, low dissolved oxygen levels, and odour in the harbour. Other contributors to the deterioration of harbour water quality include erosion of topsoil from farms, stream banks, and construction sites also contribute (Greco, 1998). Excessive nutrients, particularly phosphorus and nitrogen, result in harbour eutrophication.

Water quality problems in Hamilton Harbour are well-documented. The harbour has been categorized as the most polluted water body in North America (Gorrie, 1987). In the

1960s, the aquatic life of the harbour has been more or less entirely vanished. According to the International Joint Commission (M.O.E, 1989), in the 1970's, the harbour failed to meet the Ontario Provincial Water Quality Objectives and sediment disposal guidelines. M.O.E. (1992) reported such major problems as toxic contamination, water quality and bacterial contamination. These problems are directly related to the harbour's water. The water and sediments in the harbour are contaminated by metals (including zinc, iron, nickel, and lead) and organic compounds (including Polychlorinated biphenyls (PCB's), Polycyclic aromatic hydrocarbon (PAH's), mirex, and Dichlorodiphenyltrichloroethane (DDT)), coming from large industrial operations.

With reliable estimates of the exchange of water through the Burlington Ship Canal, we will be able to determine the hydraulic residence time of the harbour water and provide useful input to decision making with respect to water quality improvement and water pollution control. Water quality in the harbour would be drastically poorer without the exchange flow.

Without reliable estimates of the exchange of water, it would be difficult to carry out studies in other related subject areas. For example, Ling et al. (1993) used a quantitative water air sediment interaction fugacity/equivalence mass balance model to assess the fate of contaminants in the harbour. They dealt with chemicals entering and exiting the

harbour by the exchange flow. Reliable estimates of the exchange are required as the exchange flow is the most significant flow input/output for the harbour.

In summary, a good understanding of the exchange flow problem is crucial to understanding the water quality of many semi-enclosed water bodies such as harbours, bays, fjords and inlets, where the exchange with more open waters is restricted.

1.2 Thesis Objectives

The objectives of thesis are to

(1) identify processes that are important to the exchange flow through the Burlington Ship Canal, and to properly parameterize the important processes,

(2) verify an internal hydraulics model for the suitability of predicting interface profile, layer velocities and hence volume flux in each layer for channels like the Burlington Ship Canal, and

(3) provide input to practical water quality studies for Hamilton Harbour.

1.3 Scope of This Study

The remaining parts of this thesis are divided into seven chapters. Chapter Two is a review of the previous investigations on the exchange flow through the Burlington Ship

Canal and the general progress in exchange flow such as observations and theoretical analysis. In Chapter Three we introduce channel geometry and non-linear partial differential equations used to model the physical phenomena of exchange flow. In Chapter Four we concentrate on the design of simulation runs in order to capture the important characteristics of the exchange flow. In Chapter Five we present the model results for the simulation runs described in the preceding chapter, and compare the model results with experimental and field data. Chapter Six is a discussion of fluid mass exchange between Hamilton Harbour and Lake Ontario together with water quality implications. In Chapter Seven we draw conclusions based on the modelling results. Chapter Eight is a list of suggestions and recommendations for future research on exchange flow.

Chapter Two: Literature Review

The purpose of this chapter is twofold: to review previously completed research work on the exchange flow through the Burlington Ship Canal and to scrutinize assumptions and/or approximations made in exchange flow studies in general, which ought to be removed for improved calculations of fluid mass exchange.

Dick and Marsalek (1973) first noted that two flow regimes existed in the Burlington Ship Canal. The first flow regime is open-channel flow with a unidirectional velocity profile. The unidirectional flow through the canal is a result of water level difference between the two ends of the canal. The theory of open-channel flow can be found in standard textbooks (e.g. Chow, 1959; Henderson, 1966; Chaudhry, 2008).

The second flow regime is counter-flowing layered exchange of Hamilton Harbour Water and Lake Ontario Water. Recent field observations (Lawrence et al. 2004) showed that buoyant, warm water flowed out of the harbour in the upper layer, whereas in the lower layer, dense, cool lake water sank into the harbour (Figure 2.1). The field observations described the exchange for the particular conditions of summer 1996. It would be useful if we can extrapolate field results to general prevailing conditions.

Broadly speaking, the exchange flow through the canal can be observed in summer months, whereas the unidirectional flow occurs during the remainder of the year (Greco, 1998). Generally, the flow in the canal is a combination of the two regimes with a higher exchange flow component in the summer and a higher unidirectional flow component the remainder of the year.

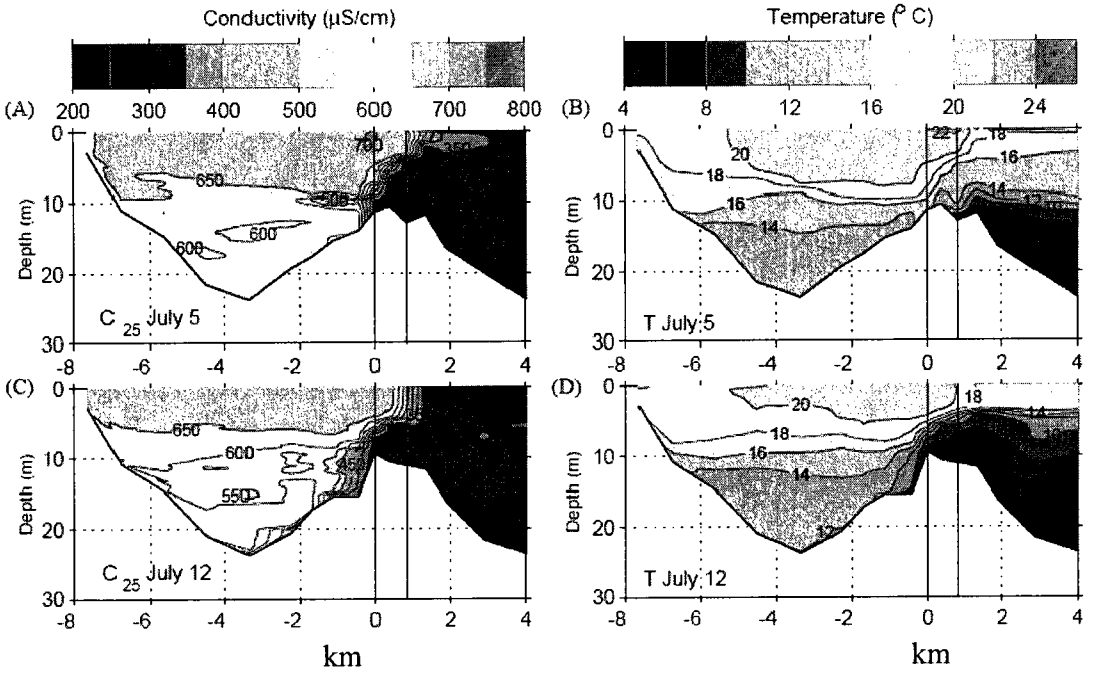

Figure 2.1: Conductivity (left panels; µS/cm at 25°C) and temperature contours along the length of Hamilton Harbour, the Burlington Ship Canal (marked by black lines) and the western end of Lake Ontario. (Adapt from Lawrence et al. 2004)

Wu et al. (1996) obtained field measurements of currents, water levels, and temperatures from Hamilton Harbour and estimated the flushing time of the harbour as three years. This estimate must be very crude, because only water-level oscillations were taken into account. On the other hand, the field results indicated that harbour water-level oscillations are important to the exchange through the Burlington Ship Canal.

The field study of Lawrence et al. (2004) is perhaps the most comprehensive one. The study evidenced that the summer exchange through the Burlington Ship Canal is qualitatively described by frictional internal hydraulic theory. At the same time, it highlighted some of the challenges in dealing with the exchange flow through the canal. Even though the canal has a simple geometry, there are many potential limitations for calculating the magnitude of the volume flux. These limitations consist of estimation of bottom and interfacial friction factors, interfacial mixing and recirculation, the presence of barotropic oscillation, and the variation in depth along and across the canal.

In an analysis of field data from the Burlington Ship Canal, Greco (1998) concluded that the two-layer flow through the canal appears to have a sharper density profile than velocity profile, although the difference is small in relation to the scatter in the data. Even though the flow is unsteady and the interface cannot be predicted with certainty, the

mixing in the canal due to interfacial instabilities is predictable. In this study, we do not attempt to include fluid mixing.

Tedford (1999) provided a detailed spectrum analysis of barotropic forcing modes that possibly influence the exchange flow through the Burlington Ship Canal. It was suggested that the barotropic flow in the canal is caused by tides and standing waves in Lake Ontario. Barotropic flow is also strongly affected by Helmholtz or Harbour resonance. The harbour exhibited Helmholtz resonance, amplifying some oscillation and damping out others. This means that the consideration of only a single-frequency barotropic forcing is probably not adequate for reliable predictions of the fluid mass exchange between Hamilton Harbour and Lake Ontario.

Hamblin and He (2003) attempted to predict the exchange using a hydrodynamics model that covers Hamilton Harbour and the western end of Lake Ontario; they encountered the difficulty to properly specify lateral open boundary conditions.

Gu and Lawrence (2005) presented an analytical solution to the problem of two-layer exchange flow for channel geometry like the canal. This solution is based on the direct integration of the fully nonlinear one-dimensional shallow-water equation including both inertial and frictional effects which are both important in determining the exchange flow rate. The results indicate dramatic exchange flow rate reductions with increasing

frictional effects. The solution indicates that the interface profile is nonlinear and asymmetric. The analytical method has assumed that the exchange is steady or independent of time.

Thus an assumption does not hold under many circumstances, including the case of the Burlington Ship Canal and other major sea straits such as the straits of Gibraltar, Bophorus, Bab-el-Mandep and Dardabelles. Density-driven exchange flows are influenced by friction, as documented in the classic work by Schijf and Schonfeld (1953) and Assaf and Hecht (1974). Exchange flows are also influenced by time-dependent barotropic forcing. To a less extent, they are influenced by mixing of fluids.

In past studies of exchange flows, researchers have introduced different levels of approximations to simplify the problem. Armi (1986) investigated the maximal exchange under steady, frictionless conditions. Armi and Farmer (1986) and Farmer and Armi (1986) analyzed frictionless exchange with quasi-steady forcing. These studies rely on solving the Bernoulli equation at some locations along the canal where the flow is controlled. In the case of frictional exchange, it is difficult to identify such locations in advance. In the case of unsteady exchange, any control point, if exist, will inevitably move back and forth along the canal in time. Thus, the aforementioned approach suffers a severe limitation, which ought to be removed.

Zaremba et al. (2003) investigated frictional effects on exchange, without barotropic forcing. Helfrich (1995) allowed for barotropic forcing, but ignored friction. Li and Lawrence (2009) considered both friction and barotropic forcing. However, the barotropic forcing considered by Helfrich (1995) and Li and Lawrence (2009) is limited to oscillations with a single fixed frequency.

Exchange flows through many sea straights are subject to barotropic forcing that features multi-frequencies (e.g. Morozov et al., 2002, Jarosz et al., 2005). In Lake Ontario, surface seiches at multiple frequencies are triggered by wind forcing, resulting in an unsteady exchange through the Burlington Ship Canal (Lawrence et al. 2004). The need to consider both friction and barotropic forcing of multiple frequencies has motivated this research.

Chapter Three: Two-layer Internal Hydraulic Model for Exchange Flow

This chapter begins with a description of model channel geometry that is pertinent to the Burlington Ship Canal. Subsequent sections cover the formulations of friction and two-layer model equations. These equations are based on mass conservation and momentum balance principle. This chapter ends with a presentation of dimensionless model equations. The main goal of the chapter is to introduce parameters that are used to conveniently represent physical processes of importance to the exchange through the canal.

3.1 Geometry

The Burlington Ship Canal has a constant width of B = 89 m, an average depth of Y = 10.6 m and a horizontal length of L = 830 m. Outwards from the two ends of the canal, the water surface of the reservoirs lake Ontario and Hamilton Harbour suddenly expands in width. We describe the width, b, of the model channel using the function given by

$$b(x)=\begin{cases} B & \text{for} -L/2 \le x \le L/2 \\ B\left|x/L\right|^{3} & \text{for} \; x<-L/2 \; \text{and} \; x>L/2 \end{cases} \tag{3.1.1}$$

where x is the horizontal coordinates. The origin is located at the midpoint of the channel

The function $b(x)$ is a smooth function, yielding smoothly matching width at $x = \pm L/2$. The choice of the lower and upper limit for x is arbitrary, solely based on the consideration of numerical stability. Using the simple shape given by b, we avoid complications arising from a more complex geometry. Thus, we can focus on the effects of friction and barotropic forcing.

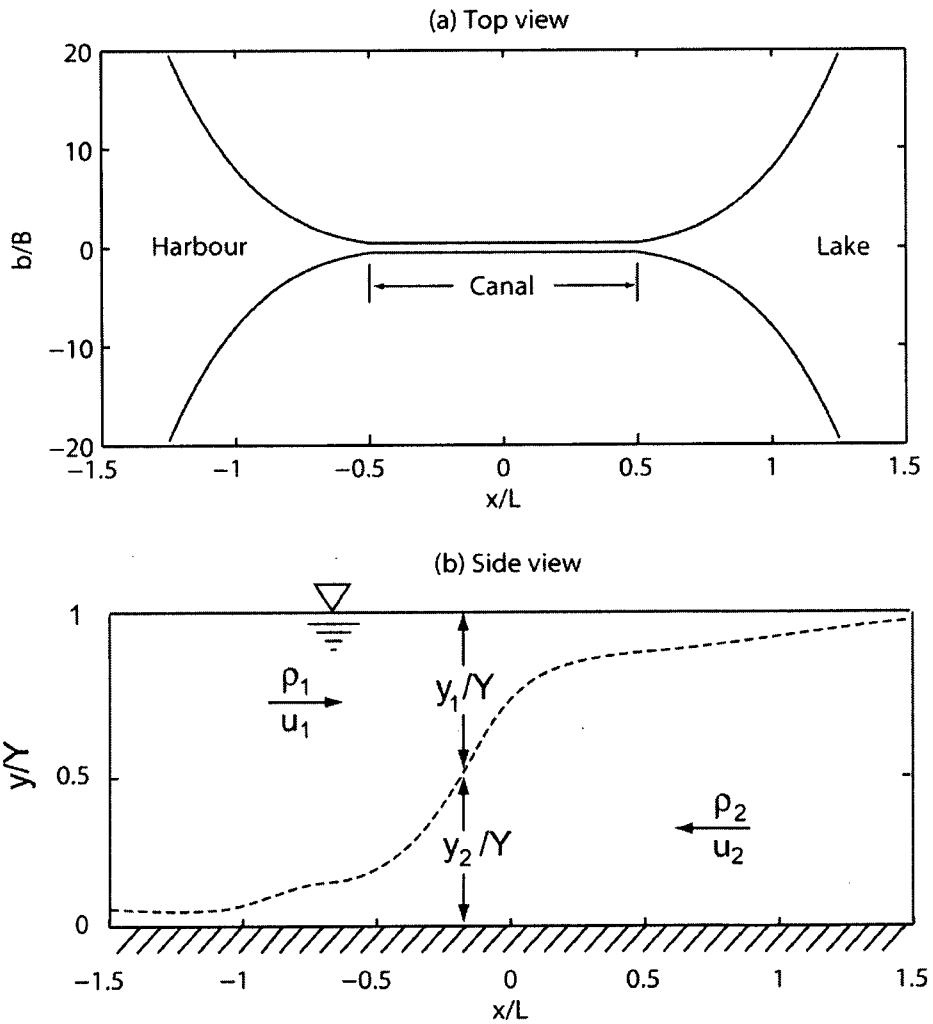

Figure 3.1: Definition diagrams of two-layer exchange flow. (a) Top view; (b) Side view. The free surface displacements are small compared with interface displacement.

In Figure 3.1, we show definition diagrams of two-layer exchange flow. The model channel has a constant width for the canal portion between x/L = -0.5 and x/L = 0.5. Outwards from the canal ends, the wdith expands like the spreading lateral edges of harbour water flowing into the lake shown in Figure 1.3. The upper and lower layer of fluids flow in opposite directions. Although there is in reality a continous variation of temparature and fluid veloity with depth, the dominant features of the motion are very close to those shown by a system with two layers of different density (Figure 3.1b).

3.2 Friction

3.2.1 Bottom friction

This section discusses the relationship between the frictional drag and the velocity near the boundary. The flow in the frictional layer is turbulent and drag law is nonlinear. The layer of flowing fluid of the upper layer contacts the sidewalls of the canal (Figure 3.2). Therefore, the motion of the upper layer is subject to friction on the sidewalls. The motion is also subject to friction at the density interface, because there is relative motion between the upper layer and the lower layer. The lower layer of flowing fluid contacts the sidewalls as well as the bottom of the canal. Thus, the motion of the lower layer is subject to friction on the canal bottom, on the sidewalls at the density interface.

Consider a fluid element in the lower layer that has a length of Δx in the along-channel direction (Figure 3.1). The height of the element is y_2. The contact area of this element with the bottom is $A = b\Delta x$. The frictional drag exerted by the bottom on the flowing fluid is given by

$$F_b = \tau_b b \Delta x \tag{3.2.1}$$

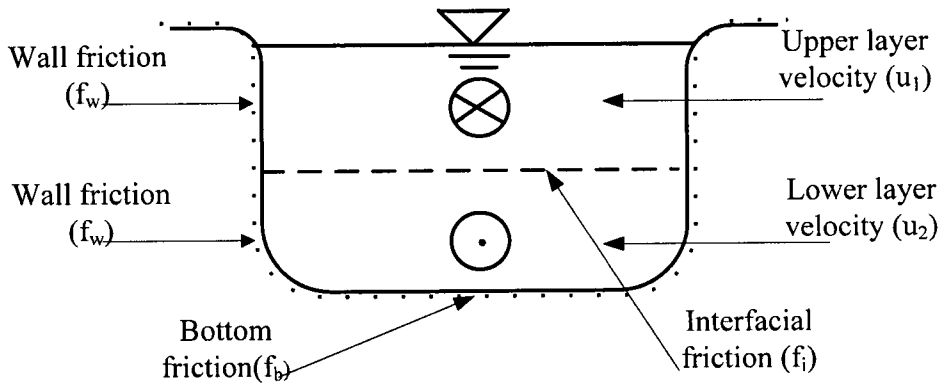

Figure 3.2: A channel cross section showing friction in two-layer exchange flow.

where τ_b is the frictional drag per unit area, due to turbulence action in the boundary layer immediately above the bottom (Figure 3.3). τ_b maybe approximated using the quadratic law, i.e, τ_b is proportional to the cross-sectional mean velocity squared.

$$\tau_b = -f_b \rho_2 u_2 |u_2| \tag{3.2.2}$$

The negative sign in equation (3.2.2) is due to the convention that a positive velocity of the lower layer is in the negative direction of the x-axis. The frictional drag acting on the fluid element is given by,

$$F_b = -f_b \rho_2 u_2 |u_2| b \Delta x \tag{3.2.3}$$

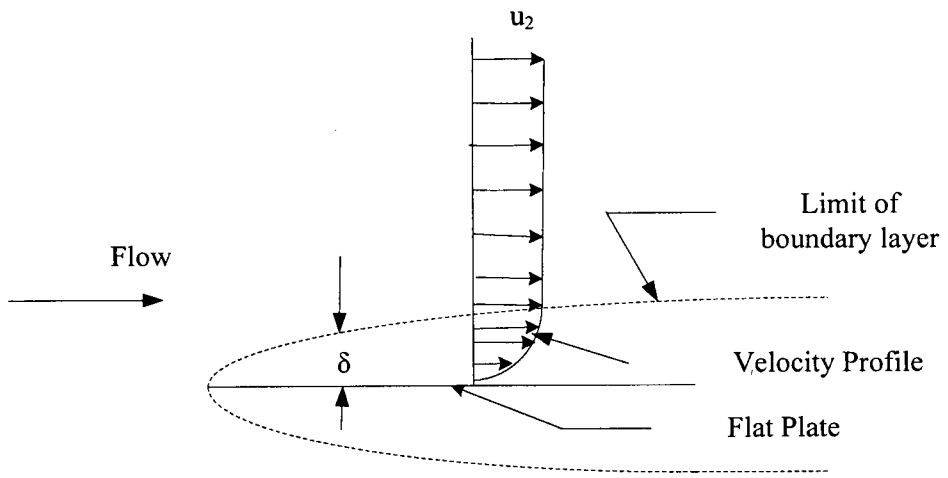

Figure 3.3: Velocity profile for flow over a flat plate.

Since the fluid element has a volume of $Vol = y_2 b \Delta x$, where b is the width of the element, the frictional drag per unit volume is given by

$$\frac{F_b}{Vol} = -\rho_2 f_b \frac{u_2 |u_2|}{y_2} \tag{3.2.3}$$

where f_b is a bottom friction factor, which can be determined by measuring turbulent shear stress and the mean flow velocity outside the boundary layer (Figure 3.3).

3.2.2 Sidewall friction

The treatment of sidewall friction is treated in a similar way as bottom friction. The contact area of an fluid element with the sidewalls is $A = y_1 \Delta x$. The frictional drag exerted by the sidewalls on the flowing fluid is given by

$$F_{1w} = \tau_w y_1 \Delta x \tag{3.2.4}$$

where τ_w is the frictional drag per unit area. Using the quadratic law for frictional drag, τ_w is given by

$$\tau_{1w} = f_w \rho u_1 |u_1| \quad \text{for the upper layer} \tag{3.2.5}$$

$$\tau_{2w} = -f_w \rho u_2 |u_2| \quad \text{for the lower layer} \tag{3.2.6}$$

where f_w is a wall friction coefficient. The drag force for the entire element due to wall friction is

$$F_{1w} = f_w \rho_1 u_1 |u_1| y_1 \Delta x \quad \text{for the upper layer} \tag{3.2.7}$$

$$F_{2w} = -f_w \rho_2 u_2 |u_2| y_2 \Delta x \quad \text{for the upper layer} \tag{3.2.8}$$

Since the fluid element has a volume of $Vol = y_1 b \Delta x$, The frictional drag per unit volume is

$$\frac{F_{1w}}{Vol} = \rho_1 f_w \frac{u_1 |u_1|}{b} \quad \text{for the upper layer} \tag{3.2.9}$$

$$\frac{F_{2w}}{Vol} = -\rho_2 f_w \frac{u_2 |u_2|}{b} \quad \text{for the lower layer} \tag{3.2.10}$$

The wall friction coefficient, f_w, can be determined in the similar way as the bottom friction factor, f_b.

3.2.3 Interfacial friction

An accurate estimate of the interfacial friction has not been established so far. Zhu and Lawrence (2000) experimentally determined the interfacial friction factor based on the principle of energy conservation. Using the measured exchange flow rate and density interface position along the channel, the interfacial friction factors were evaluated by integrating the energy equation. The frictional drag per unit volume of fluid element is given by

$$\frac{F_{1i}}{Vol} = \rho_1 f_i \frac{u_1|u_1|}{y_1} \qquad \text{for the upper layer} \qquad (3.2.11)$$

$$\frac{F_{2i}}{Vol} = -\rho_2 f_i \frac{u_2|u_2|}{y_2} \qquad \text{for the lower layer} \qquad (3.2.12)$$

3.3 Governing Equations

3.3.1 Assumptions

A number of major approximations are made in modelling many flows of geophysical, oceanographic, meteorological, and engineering importance as two-layer flows. Through

the approximations, we simply the problems of exchange flow but still retain the important physics at work. The major approximations made in this study are:

(1) No fluid mixing occurs across the density interface, which means that the fluid density within each layer remains constant. This eliminates the need to calculate density change.

(2) Hydrostatic pressure is assumed.

(3) The flow is one-dimensional, with layer velocities varying only in the flow direction.

(4) A small relative density difference between the layers is assumed, ensuring an element horizontal free surface and allowing us to focus on variations in interface height.

To some extent, fluid mixing does occur at the density interface due to turbulent motion. The mixed fluids of the upper and lower layer will have temporally and spatially varying densities between ρ_1 and ρ_2. To predict such density variations is beyond the scope of this study.

The hydrostatic pressure approximation is acceptable in studies of exchange flow as the flow is mainly in the horizontal direction. The fluid acceleration in the vertical is expected to be small, except where a hydraulic jump takes place, which is possible. From

the length scale perspective, the horizontal length scale is very much larger than the vertical length scale, with L = 830 (m) and Y = 10.6 (m). This disparity between the horizontal and vertical length scales makes the hydraulic approximation a valid approximation.

Within the canal the flow is confined by the two sidewalls. We can expect the fluid velocity in the cross canal direction to be much smaller than that in the along-canal direction. Therefore, the one-dimensional flow approximation is reasonable, as far as the flow within the canal is concerned. This approximation may not hold at sudden expansions at the canal's ends. However, it is the flow within the canal that is interesting to us. The aforementioned approximations are introduced to the model equations presented below.

3.3.2 Continuity Equations

For the upper layer of fluid, the equation of continuity can be written as

$$\frac{\partial a_1}{\partial t} + \frac{\partial}{\partial x}(a_1 u_1) = 0 \qquad (3.3.1)$$

where subscript 1 is used for the upper layer, a_1 is the cross-sectional area at a given location in the channel, t is the time, and u_1 is the fluid velocity. The first term on the left

hand side is an unsteady term that describes the time rate of cross-sectional area change (in m^2/s). In the second term, a_1u_1 represents the volumetric flux (in m^3/s).

Consider a fluid element, which is bounded by the free surface on the top, the density interface on the element's bottom, the two sidewalls of the channel on the sides, a lateral surface in the downstream and a lateral surface in upper. If there is a net gain of volume flux through the lateral surfaces into the element, $\frac{\partial}{\partial x}(a_1u_1)$ will be negative. As a result, $\frac{\partial a_1}{\partial t}$ will be positive, meaning that the density interface of the element will move downwards. On the other hand, if there is a net loss of volume flux from the element, $\frac{\partial}{\partial x}(a_1u_1)$ will be positive, and therefore $\frac{\partial a_1}{\partial t}$ will be negative. This means that the density interface of the element will move upwards.

For the lower layer, the equation of continuity is given by

$$\frac{\partial a_2}{\partial t}+\frac{\partial}{\partial x}(a_2u_2)=0 \qquad (3.3.2)$$

where t subscript 2 is used for the lower layer. This equation can be interpreted in the same way as that for the upper layer. The above equation of continuity (3.3.2) is presented for completeness only. In fact, once the cross sectional area of the upper layer is obtained from solving partial differential equations, the cross sectional area of the lower layer at any location in the channel can be determined algebraically as the

difference between the total cross sectional area, bY, of the channel and the cross sectional area of the upper layer, i.e.

$$a_2 = bY - a_1 \tag{3.3.3}$$

This is an approximation, which is valid due to the fact that the free surface displacements are small, relative to the interface displacement (Figure 3.1b). We emphasize that under many circumstances, exchange flow exhibits time-dependent volume fluxes through the upper and lower layer. Therefore, the density interface will move up and down in time, as is the case in the exchange flow through the Burlington Ship Canal.

3.3.3 Momentum Equations

The momentum balance equations for a two-layer system are based on Newton's second law of motion. Following Li and Lawrence (2009), for the upper layer, we write the momentum balance equation as

$$\frac{\partial u_1}{\partial t} + \frac{\partial}{\partial x}\left[u_1^2/2 + g(y_1 + y_2)\right] = g'(S_{1w} + S_{1i}) \tag{3.3.4}$$

where g is the gravity, and g' is the reduced gravity defined as

$$g' = g(\rho_2 - \rho_1)/\rho_2 \tag{3.3.5}$$

In the definition, ρ_1 is the density of the upper layer fluid and ρ_2 is the density of the lower layer fluid.

The first term on the left hand side of equation (3.3.4), $\frac{\partial u_1}{\partial t}$, is unsteady term or local acceleration (in m/s^2). In the second term on the left hand side, $\frac{\partial}{\partial x}\left(u_1^{\,2}/2\right)$ represents advective acceleration or non-liner acceleration (in m/s^2); $\frac{\partial}{\partial x}[g(y_1+y_2)]$ is the horizontal gradient of fluid pressure that is assumed to be hydraulic static; this is the pressure force (in N/kg or force per unit mass of fluid) acting on a fluid element of interest.

The term on the right hand side of the equation (3.3.4) is the sum of the stresses (in Newton per unit mass of fluid) due to sidewall friction, S_{1w}, and interface friction, S_{1i}. Both act to retard the upper layer of flowing fluid. It is assumed that friction on the water surface is negligible. Note that bottom friction does not directly affect the upper layer fluid.

The friction on the sidewalls is given by

$$S_{1w} = -f_w \frac{u_1|u_1|}{g'b} \tag{3.3.6}$$

If u_1 is positive, S_{1w} will be negative and vice versa. To understand the way sidewall friction works, we consider the balance between the terms

$$\frac{\partial u_1}{\partial t} \text{ and } -f_w \frac{u_1|u_1|}{g'b}$$

in the momentum balance equation (3.3.5). If $u_1 > 0$ or the upper layer is flowing from left to right the friction term is negative, $\frac{\partial u_1}{\partial t}$ will be negative or u_1 decreases in time, meaning that the left-to-right flowing fluid slows down due to sidewall friction. On the other hand, if $u_1 < 0$ or the upper layer is flowing from right to left the friction term is positive, $\frac{\partial u_1}{\partial t}$ will be positive or u_1 increases in time. An increase in u_1 in time is in the sense that sidewall friction causes the upper layer to flow from left to right, which is equivalent to slow down the right-to-left flowing fluid. This explains the retarding nature of sidewall friction on the upper layer of flowing fluid.

The S_{1w} function states that the sidewall friction is inversely proportional to the width of the channel. That is to say that sidewall friction becomes less important with increasing channel width. In the case of Burlington Ship Canal, there is a sudden increase in water surface width outwards from the canal ends. Thus, sidewall friction outside the canal ends is expected to be much less significant than sidewall friction within the canal, where the flowing fluids are more confined.

The friction at the interface is given by

$$S_{1i} = \frac{f_i}{2} \frac{\Delta u|\Delta u|}{g'y_1} = \frac{f_i}{2} \frac{(u_2 - u_1)|u_2 - u_1|}{g'y_1} \qquad (3.3.7)$$

where Δu is defined as $\Delta u = u_2 - u_1$ We can interpret the friction term in the following way. If the exchange flow is steady, the lower layer flows from right to left or $u_2 < 0$, whereas the upper layer flows from left to right or $u_1 > 0$. Then, $S_i < 0$. In this case, the retarding effect of interfacial friction on the upper layer can be explained in the same way as that of the sidewall friction. For other flow cases, the effect of the interfacial friction can be explained in a similar way.

It is important to note that if the upper layer becomes excessively thin at some locations in the model channel during a simulation run, the function S_{1i} will yield very large values for the interfacial friction term. Such an occurrence will cause the simulation run to be unstable. Physically, neither the upper nor the lower layer can be very thin, because an excessively thin layer will be destroyed by turbulent shear.

We do not attempt to model the physical processes that result in interfacial shear, but retain their gross effect on the momentum balance of the flowing layers, using the quadratic friction law. The interfacial friction is inversely proportional to the upper layer thickness y_1. Bottom friction and sidewall friction are treated similarly. With these simplifications, two-layer exchange is completely described by interface height and layer velocities.

For the lower layer, the momentum balance equation is written as

$$\frac{\partial u_2}{\partial t}+\frac{\partial}{\partial x}\left[u_2^2/2+g(y_1+y_2)-g'y_1\right]=g'(S_b+S_{2w}+S_{2i}) \tag{3.3.8}$$

The first term on the right hand side, $\frac{\partial u_2}{\partial t}$, is an unsteady term or local acceleration. In the second term, $\frac{\partial}{\partial x}\left(u_2^2/2\right)$, is a nonlinear acceleration or advective acceleration, and $\frac{\partial}{\partial x}\left[g\left(y_1+y_2\right)-g'y_1\right]$ is the pressure gradient. The term on the right hand side of equation (3.3.8) is the sum of frictional stresses (in Newton per unit fluid mass) due to bottom friction, sidewall friction and interfacial friction. All of them work to retard the motion of the lower layer fluid, which is similar to the friction terms for the upper layer.

Bottom friction is given by

$$S_b=-f_b\frac{u_2|u_2|}{g'y_2} \tag{3.3.9}$$

This function states that bottom friction is proportional to the lower layer velocity squared and inversely proportional to the lower layer thickness y_2. The thicker the lower layer, the less significant is the bottom friction. On the other hand, if the lower layer is too thin somewhere in the model channel during a simulation run, the simulation can become unstable because of excessively large values for the bottom friction term. Bottom friction does not affect the upper layer since they do not come to contact with each other.

Sidewall friction is given by

$$S_{2w}=-f_w\frac{u_2|u_2|}{g'b} \tag{3.3.10}$$

The functional form is the same as sidewall friction for the upper layer. Therefore, discussions about the effect of sidewall friction on the upper layer are also relevant to the lower layer.

The interface friction term in the momentum balance equation (3.3.8) for the upper layer is given by

$$S_{2i} = -\frac{f_i}{2}\frac{\Delta u|\Delta u|}{g' y_2} \tag{3.3.11}$$

Interfacial friction is inversely proportional to the lower layer thickness y_2. The function form is the same as that for the upper layer, but the sign is opposite.

In summary, among the continuity equations (3.3.1), (3.3.2) and the momentum equations (3.3.4), (3.3.8) there are four unknown dependent variables, namely a_1, a_2, u_1, and u_2. In principle, for given parameters, coefficients, channel geometry, initial conditions and open boundary conditions, we can solve the model equations for the four unknowns. Once a_1 and a_2 throughout the entire model channel are solved, y_1 and y_2 can be obtained algebraically as follows

$$y_1(x) = \frac{a_1(x)}{b(x)} \tag{3.3.12}$$

and

$$y_2(x) = \frac{a_2(x)}{b(x)} \tag{3.3.13}$$

Thus, complete solutions of the layer velocities and interface positions over the entire model channel are obtained. However, it is desirous to reduce the number of unknowns, which will simplify the solution procedures.

3.3.4 Relationship between velocity shear and layer velocities

Following Helfrich (1995), we introduce velocity shear defined as the difference between the lower and upper layer velocity, i.e.

$$u_2 - u_1 = \Delta u \tag{3.3.14}$$

Instead of seeking solutions for two unknowns u_1 and u_2 from the momentum balance equations, we combine the two equations to yield a partial differential equation for Δu. This equation will be derived later.

In order to recover the layer velocities from the velocity shear, we introduce volumetric flux, q, (m^3/s), which is based on depth-average from the surface to the bottom flow and which is referred to as barotropic volumetric flux. If the depth-average fluid velocity through the model channel is u_o, the total depth of flow is Y and the channel width is b, we can calculate q from

$$q = u_o Y b \tag{3.3.15}$$

Usually, u_o is time-dependent and is determined using field measurements made from a channel of interest. Measurements of Y and b can be readily made. Therefore, the barotropic volume flux is known, as a function of time.

On the other hand, the volumetric flux based on layer velocities and thicknesses is the sum of $u_1 a_1$ and $u_2 a_2$ (in m^3/s). This sum must be equal to the volumetric flux based on the depth-average flow, meaning that

$$u_1 a_1 + u_2 a_2 = q \tag{3.3.16}$$

Between the velocity shear definition (3.3.14) and equation (3.3.16), we can determine the layer velocities as follows

$$u_1 = \left[(q + a_1 \Delta u)/a\right] - \Delta u \tag{3.3.17}$$

$$u_2 = \Delta u + u_1 \tag{3.3.18}$$

where a is the total cross-sectional area of the channel or $a = bY$.

In the special case where there is zero depth-average volume flux or $q = 0$, the volume flux through the upper layer, $u_1 a_1$ is the same as that through the lower layer $u_2 a_2$, except that the flow is in the opposite direction to each other. The layer velocities will be

$$u_1 = \frac{a_1}{a}\Delta u - \Delta u \tag{3.3.19}$$

$$u_2 = \Delta u + u_1 \tag{3.3.20}$$

The layer velocities are needed for evaluations of the friction terms in the momentum balance equation and for evaluations of exchange fluxes in each layer.

A partial differential equation for velocity shear is derived by subtracting the momentum balance equation (3.3.4) for the upper layer from the momentum equation (3.3.8) for the lower layer. The resultant equation is given by

$$\frac{\partial \Delta u}{\partial t} + \frac{\partial}{\partial x}\left(\frac{u_2^{\,2} - u_1^{\,2}}{a} - g' y_1 \right) = g'\left(S_b + S_{2w} + S_{2i} - S_{1w} - S_{1i}\right) \tag{3.3.21}$$

With substitutions of the friction terms and use of $Y = y_1 + y_2$, the above equation for Δu becomes

$$\begin{aligned} \frac{\partial \Delta u}{\partial t} + \frac{\partial}{\partial x}\left(\frac{q\Delta u + a_1 \Delta u^2}{a} - \frac{\Delta u^2}{2} - g' y_1 \right) = \\ - g'\left(f_b \frac{u_2 |u_2|}{2 y_2} + f_i \frac{Y \Delta u |\Delta u|}{2 y_1 y_2} + f_w \frac{u_2 |u_2| - u_1 |u_1|}{b} \right) \end{aligned} \tag{3.3.22}$$

3.4 Scales

It is preferred to convert the dimensional model equations into non-dimensional equations, which can be conveniently applied to different channels and straits where exchange flows take place. Applications to different sites will have different values for parameters associated with channel geometry, friction coefficients and barotropic forcing, but the dimensionless model equations will remain the same. It has been clarified that

only a_1 and Δu need to be solved from the two partial differential equations (3.3.1) and (3.3.22). Other dependent variables can be determined algebraically. Therefore, non-dimensionalization will be carried out for the two equations. For this purpose, we need to choose the appropriate scales for time, length, fluid velocity and volume flux.

3.4.1 Time scale

We choose the time period, T, of barotropic forcing as the time scale. Thus, independent variable t in equations (3.3.1) and (3.3.22) is substituted by Tt^*. This is to say that we introduce dimensionless time t^* as

$$t^* = t/T \tag{3.4.1}$$

This choice is justified by the consideration that the purpose of this study is to investigate the exchange flow influenced by time-dependent barotropic forcing. Barotropic forcing can consist of more than one mode with different time periods. For example, different modes of the barotropic forcing that influence the exchange flow through the Burlington Ship Canal have time period, T, ranging 2.7 to 12.5 hours, as determined from field observations made within the canal and the nearby waters (Tedford, 1999). It would be interesting to examine the behaviour of the exchange flow through the canal in response to each of the modes.

3.4.2 Length scales

There are three length scales involved, namely a horizontal length scale in the along-channel direction, a horizontal length scale in the cross-channel direction and a vertical length scale. For the horizontal length scale in the along-channel direction, we choose the length of the channel, L. Thus, the x coordinates in the model equations is normalized by

$$x^* = x / L \tag{3.4.2}$$

x^* is dimensionless.

For the horizontal length scale in the cross-channel direction, we choose the width of the channel, B. This is because the channel geometry is expected to exert influence on the exchange flow. The width, b, in the model equations is normalized by

$$b^* = b / B \tag{3.4.3}$$

b^* is dimensionless. It is equal to one within the Burlington Ship Canal and larger than one outwards from the two canal ends.

For the vertical length scale, we choose the total depth of the flow in the canal. The upper and lower layer thicknesses are normalized as follows

$$y_1^* = y_1 / Y$$

(3.4.4)

$$y_2^* = y_2 / Y \tag{3.4.5}$$

y_1^* and y_2^* are dimensionless.

Y is the only logical choice, since we are interested in the flow within the channel. It makes sense to use the total depth of flow in the channel as the vertical length scale.

3.4.3 Velocity and volume flux scales

Experimental and field data provide evidence that the fluid velocity of density-driven exchange flow is proportional to $\sqrt{g'}$. $\sqrt{g'Y}$ has the dimension of velocity. We choose it as the velocity scale for both the velocity shear and the layer velocities. The dimensionless velocity shear, upper-layer velocity and lower-layer velocity are, respectively,

$$\Delta u^* = \frac{\Delta u}{\sqrt{g'Y}} \tag{3.4.6}$$

$$u_1^* = \frac{u_1}{\sqrt{g'Y}}$$

(3.4.7)

$$u_2^* = \frac{u_2}{\sqrt{g'Y}} \tag{3.4.8}$$

physically, $\sqrt{g'Y}$ represents the phase speed at which interfacial waves propagate through the canal. We have assumed that the fluid velocities of the upper and lower layers have the same scale as the velocity shear

The appropriate volume flux scale is $u_0 YB$. In other words, q is normalized by

$$q^* = q/(u_o YB) \tag{3.4.9}$$

q^* is dimensionless

u_o is the amplitude of depth-average flow speed, which is to be obtained from field measurements.

3.5 Dimensionless model equations

Using the dimensionless independent and dependent quantities introduced in Section 3.4, we obtain the dimensionless form of equations (3.3.1) and (3.3.22), given by

$$\frac{\partial a_1^*}{\partial t^*} + \gamma \frac{\partial}{\partial x^*}\left(\frac{\beta q^* a_1^* + a_1^{*2}\Delta u^*}{a^*} - a_1^* \Delta u^* \right) = 0 \tag{3.5.1}$$

$$\frac{\partial \Delta u^*}{\partial t^*} + \gamma \frac{\partial}{\partial x^*}\left(\frac{\beta q^* \Delta u^* + a_1^* \Delta u^{*2}}{a^*} - \frac{\Delta u^{*2}}{2} - y_1^* \right) = -\gamma\alpha\left(\frac{u_2^* |u_2^*|}{2y_2^*} + r_i \frac{y^* \Delta u^* |\Delta u^*|}{2y_1^* y_2^*} + r_w \frac{u_2^* |u_2^*| - u_1^* |u_1^*|}{b^*} \right) \tag{3.5.2}$$

Five dimensionless parameters appear in equations (3.5.1) and (3.5.2):

$$\alpha = f_b \frac{L}{Y} \tag{3.5.3}$$

$$\beta = \frac{u_\circ}{\sqrt{g'Y}} \tag{3.5.4}$$

$$\gamma = \frac{T}{L/\sqrt{g'Y}} \tag{3.5.5}$$

$$r_i = \frac{f_i}{f_b} \tag{3.5.6}$$

$$r_w = \frac{f_w Y}{f_b B} \tag{3.5.7}$$

where f_w, f_b and f_i are the side wall, friction coefficient bottom friction coefficient, and interfacial friction coefficient, respectively. The three primary parameters can be interpreted in the following way:

(1) α measures the relative importance of frictional effects to inertial effects;

(2) β measures the strength of the barotropic flow relative to the velocity scale of the density-driven flow; and

(3) γ represents the ratio of the forcing period to the time scale for interface waves to travel through the canal.

For time-dependent exchange flow, we need to solve the partial differential equations over the entire model channel. This is different from the steady, frictionless case where we have prior knowledge regarding the location where the flow is controlled; in this simple case we may apply the Bernoulli equation at the control point, at which there is a fixed relationship between the flow velocity and flow depth. In the time dependent case, any control point, if exist, may move back and forth along the channel.

The Reynolds number, *Re*, is a dimensionless number that is the ratio of inertial force to viscous force. It measures the relative importance of the two forces:

$$Re = \frac{VY}{\nu} \tag{3.5.8}$$

where V is maximum layer-velocity ($V \approx 0.424$ m/s), Y is total depth ($Y = 10.6$ m), and ν is kinematic viscosity ($\nu = 1.004 \times 10^{-6}$ m^2/s at 20C°). The Reynolds number is approximately 4×10^6, therefore the flow is turbulent. The above values are for the Burlington Ship Canal.

3.6 Barotropic forcing

Barotropic flow is caused by water surface gradients along the axis of the canal. These gradients are a result of water level oscillations in Lake Ontario or Hamilton Harbour, causing depth-independent, back-and-forth flow through the canal. Strong currents independent of depth were observed in the Burlington Ship Canal (Dick and Marsalek, 1973; Palmer and Poulton, 1976; Fox et al., 1996). The water levels in the canal inevitably oscillate. However, we neglect such oscillations over the short distance of the canal for simplification. This simplification means that the water surface in the canal remains flat all the time. The oscillations in the vicinity of the canal have been attributed to the possibilities of standing waves, tidal oscillations and Helmholtz resonance, as discussed in Tedford (1999).

3.6.1 Standing waves

Standing waves occur in enclosed or semi-enclosed basins (e.g. Hamilton Harbour) and are the result of the combination of incident waves (e.g. waves propagating from Lake Ontario towards Hamilton Harbour) on to a vertical boundary (e.g. the southwest end of the harbour) and their reflected waves (waves travelling from the harbour toward the lake). The period of these oscillations is the same as the incident waves. These are long, low-amplitude waves travelling at a phase speed of $c = \sqrt{gY}$. The wavelength of theses waves is so long that the Burlington Ship Canal is just a small portion of the wavelength. Therefore, the fluid particle velocities associated with these waves are considered to be the same throughout the canal, and from the water surface to the canal bottom.

The time period of standing waves is given by

$$T_n = \frac{2L}{n\sqrt{gY}} \tag{3.6.1}$$

where n is the number of wave nodes over the length of the canal (Figure 3.4). In the past, Rao and Schwab (1976) have examined standing waves in Lake Ontario. Wu et al. (1997) have investigated standing waves in Hamilton Harbour. Palmer and Poulton (1976) provided field evidence of standing wave oscillations from velocity measurements from the canal.

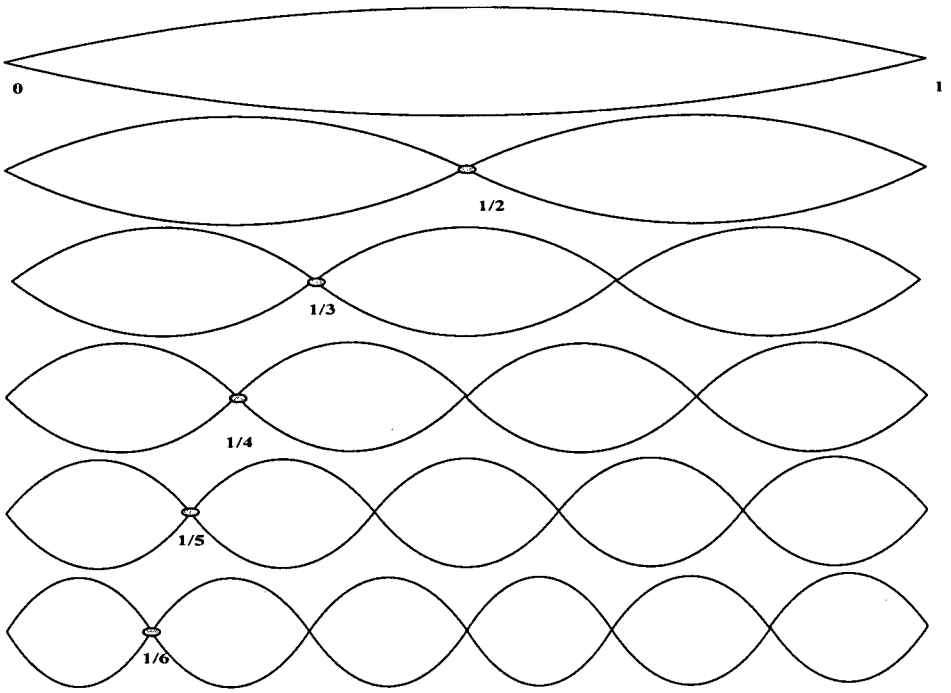

Figure 3.4: Modes of standing waves.

3.6.2 Tidal oscillations

Tidal oscillations were observed in the Great Lakes by Hutchinson (1957). These oscillations are associated with the orbital motion of the moon, and to a lesser extent that of the earth and the sun, which influence the surface of large water bodies at regular periods. The most important tidal component is often the semi-diurnal lunar tides of 12.42 hour time period (Hanson, 1960).

3.6.3 Helmholtz resonance

Helmholtz resonance is the phenomenon of air resonance in a cavity. Freeman et al. (1974) noted co-oscillations or Helmholtz resonance between Lake Ontario and Hamilton Harbour. Helmholtz resonance occurs where a harbour is connected to another water body subject to surface oscillations. An analogy with a common forced and damped particle oscillator is useful in understanding this source of current in the canal.

3.6.4 Single frequency forcing

In Helfrich (1995) and Li and Lawrence (2009), barotropic forcing was introduced via a volume flux of a single fixed frequency and amplitude:

$$q = q_{\circ} \sin(2\pi t / T) \tag{3.6.2a}$$

or equivalently

$$u_b = u_{\circ} \sin(2\pi t / T) \tag{3.6.2b}$$

where u_b is the known velocity of barotropic or depth-average flow. The dimensionless form of the volume flux is

$$q^* = \sin(2\pi t^*) \tag{3.6.3}$$

Barotropic forcing typically consists of components of different frequencies. Some or all may be significant. It is likely to consider barotropic forcing of multi-frequencies of the form

$$q = \sum_n q_n \sin(2\pi t / T_n + \theta_n) \tag{3.6.4}$$

where q_n, T_n and θ_n are the amplitude, time period and initial phase of the n'th mode of barotropic forcing, respectively. Without a loss of generality, we may set θ_1 to zero. The initial phase $\theta_2, \theta_3 \cdots \theta_n$ of the other components will be relative to the phase of the first mode. In the present study, we implement barotropic forcing modes individually.

In the model, barotropic forcing is implemented through the volume flux given in equation (3.4.9). Barotropic forcing causes depth-independent flow, i.e. the velocity would be the same from the water surface to the channel bottom. This is different from density-driven flow. Density-driven flow varies from the surface to the bottom like exchange flow, with the upper and lower layers flowing in opposite directions.

Chapter Four: Design of Simulation Runs

In the preceding chapter we have presented a system of nonlinear partial differential equations of the first order, with additional algebraic relationships that are necessary. It is not feasible to obtain analytical solutions to these equations, for given initial and boundary conditions. Li and Lawrence (2009) have discussed approximation methods appropriate for the equations. The finite difference code for implementing the approximation methods is available to us in this study. In this chapter our focus is on the design of

- sensitivity test runs,
- laboratory channel simulations, and
- Burlington Ship Canal simulations.

4.1 Sensitivity test runs

We are interested in model results for the canal portion ($-0.5 < x/L < 0.5$) of the model channel (Fig. 3.1a). It is important to avoid undesirable channel end effects on the model results for the canal portion. The simplest way to do so will be to place the channel open boundaries beyond $x/L = \pm 0.5$. The question is how far beyond the boundaries

should be placed to satisfy the above-mentioned requirement and at the same time to avoid excessive computational cost. Note that since the model channel expands rapidly in width beyond $x/L = \pm 0.5$ (Fig. 3.1a), we make the assumption that the flow is uniform in the cross-channel direction which may not hold if the model channel extends too far beyond $x/L = \pm 0.5$.

To answer the above-mentioned question, a total of nine sensitivity test runs (Table 4.1.1) are performed without barotropic forcing, i.e. $\beta = 0$. The nine sensitivity runs are divided into three groups. Group one (SM1, SM2 and SM3) uses moderate friction ($\alpha = 0.3$), group two (SS1, SS2 and SS3) uses strong friction ($\alpha = 1.57$), and group three (SW1, SW2 and SW3) uses weak friction ($\alpha = 0.03$).

In group one (SM1, SM2 and SM3), the runs use identical values for all friction parameters, but differ in the length of model channel (Table 4.1.1). The model channel (Fig. 3.1a) extends from x/L = -1 to 1 for run SM1, from x/L = -1.5 to 1.5 for run SM2, and from x/L = -2 to 2 for run SM3. The friction parameters are $\alpha = 0.30$, $r_i = 1$ and $r_w = 0.12$, respectively.

The reason for choosing these friction parameter values is given below. Dick and Marsalek (1973) obtained estimates of the bottom friction coefficient $f_b = 0.0039$ from estimates of Manning's n values for the Burlington Ship Canal. The corresponding value

for the bottom friction parameter will be $\alpha = 0.30$, as calculated from L = 830 m, Y = 10.6 m, using equation (3.5.3). According to Lawrence et al. (2004) and Gu and Lawrence (2005), the interface friction coefficient is $f_i = 0.004$, giving $r_i = 1$

Table 4.1.1: Parameter values for sensitivity runs

Run	α	r_i	r_w	Domain length
SS1	1.57	1	0.12	$-1 < x / L < 1$
SS2	1.57	1	0.12	$-1.5 < x / L < 1.5$
SS3	1.57	1	0.12	$-2 < x / L < 2$
SM1	0.30	1	0.12	$-1 < x / L < 1$
SM2	0.30	1	0.12	$-1.5 < x / L < 1.5$
SM3	0.30	1	0.12	$-2 < x / L < 2$
SW1	0.03	1	0.12	$-1 < x / L < 1$
SW2	0.03	1	0.12	$-1.5 < x / L < 1.5$
SW3	0.03	1	0.12	$-2 < x / L < 2$

[equation [3.5.6)]. We assume that the sidewall friction coefficient is the same as the bottom friction coefficient, i.e. $f_w = 0.0039$, and therefore the sidewall friction parameter is $r_w = 0.12$ [equation (3.5.7)]. No surface friction is present in these runs. Friction with $\alpha = 0.30$ may be termed moderate friction.

In group two (SS1, SS2 and SS3), the friction parameters for the three runs are the same, with $\alpha = 1.57$, $r_i = 1$ and $r_w = 0.12$. These values are based on the literature friction

coefficient of $f_b = f_w = 0.02$ and $f_i = 0.02$. The model channel (Fig. 3.1a) extends from x/L = -1 to 1 for run SS1, from x/L = -1.5 to 1.5 for run SS2, and from x/L = -2 to 2 for run SS3.

In group three (SW1, SW2 and SW3), the friction parameters are: $\alpha = 0.03$, $r_i = 1$ and $r_w = 0.12$. The friction parameter α is lower than that in the group one friction, by an order of magnitude. The model channel (Fig. 3.1a) extends from x/L = -1 to 1 for run SW1, from x/L = -1.5 to 1.5 for run SW2, and from x/L = -2 to 2 for run SW3.

The width of the model channel is given by equation (3.1.1) for all the sensitivity runs. These runs proceed until a state of equilibrium is reached.

4.2 Laboratory channel simulations

A total of sixteen simulation runs (Table 4.2.1) were conducted for comparisons with laboratory experiments of steady exchange flow, reported in Gu and Lawrence (2005). The laboratory experiments used a straight, rectangular channel of L = 2 m long and B = 0.152 m wide. Through the experiments the total fluid depth was constant at Y = 0.28 m (Gu and Lawrence 2005). Estimates of the bottom friction coefficient, f_b, were obtained using the methodology of Zhu and Lawrence (2000). The estimates of f_b range from 0.0071 to 0.0132. From the values for f_b, L and Y, we obtained estimates of the bottom

friction parameter α from equation (3.5.3). Analysis of the experiments yielded the interfacial friction coefficient, f_i, equal to $0.33f_b$, i.e. $r_i = 0.33$ [equation (3.5.6)] The laboratory experiments were steady without barotropic forcing. Thus, $\beta = 0$.

Table 4.2.1: Parameter values for steady simulation runs LC1 to LC16, which match the conditions of the laboratory experiments of Gu and Lawrence (2005). There are no surface friction and barotropic forcing for these runs.

Run	α	r_i	r_w	*Run*	α	r_i	r_w
LC1	0.094	0.33	0.92	LC9	0.094	0.33	1.84
LC2	0.091	0.33	0.92	LC10	0.091	0.33	1.84
LC3	0.083	0.33	0.92	LC11	0.083	0.33	1.84
LC4	0.077	0.33	0.92	LC12	0.077	0.33	1.84
LC5	0.074	0.33	0.92	LC13	0.074	0.33	1.84
LC6	0.068	0.33	0.92	LC14	0.068	0.33	1.84
LC7	0.059	0.33	0.92	LC15	0.059	0.33	1.84
LC8	0.051	0.33	0.92	LC16	0.051	0.033	1.84

The experiments did not provide estimates of the sidewall friction coefficient, f_w. However, the sidewall friction is expected to be important, because the laboratory channel is narrow relative to the total depth of flow. The ratio of the total depth to the channel width is $Y/B = 1.84$. To determine r_w [equation (3.5.7)], we consider two cases: $f_w = 0.5f_b$ and $f_w = f_b$. The resultant values for r_w are listed in Table 4.2.1. The sixteen

simulation runs listed in Table 4.2.1 are steady runs without barotropic forcing. Simulation runs LC1 to LC8 correspond to $f_w = 0.5f_b$, and simulation runs LC9 to LC16 correspond to $f_w = f_b$. The sixteen simulation runs differ in bottom friction and/or sidewall friction.

The main goal of the sixteen simulation runs is to confirm the suitability of the two-layer model for controlled laboratory conditions so that we can have confidence in the model results when implementing the model to field conditions. The laboratory channel has the same shape as the Burlington Ship Canal. The reduced gravity of the laboratory experiments is in the same range as that between Hamilton Harbour and Western Lake Ontario.

4.3 Burlington Ship Canal simulations

As mentioned earlier, friction with $\alpha = 0.30$ may be termed moderate friction. Since large uncertainties exist in estimates of f_b, it would be constructive to consider the possibilities of weak and strong friction, characterized by $\alpha < 10^{-1}$ and $\alpha > 10^{0}$, respectively. Simulation runs with strong, moderate, and weak bottom friction are described below.

4.3.1 Strong friction simulations ($\alpha > 10^0$)

For simulation runs with strong friction, we use the literature values of $f_b = f_w = 0.02$ and $f_i = 0.02$. The value of the bottom friction coefficient is based on the study of Zhu and Lawrence (2000). The bottom friction parameter will be $\alpha = 1.57$, as estimated from L = 830 m and Y = 10.6 m. Friction with $\alpha > 1$ is termed high friction. The interfacial friction parameter is r_i = 1 [equation (3.5.6). The sidewall friction parameter is r_w = 0.12 [equation (3.5.7)]. The barotropic forcing parameters are the same as the moderate friction runs. Table 4.3.1 lists all the parameter values for the high friction simulations.

Table 4.31: Parameter values for runs BSF1–BSF7. There is no surface friction in all the runs. Barotropic forcing in runs BSF1–BSF7 corresponds to the average of the oscillation modes described in Hamblin (1982) and Tedford (1999).

Run	T (hr)	u_0 (cm/s)	α	r_i	r_w	β	γ
BSF1	3.2	22.4	1.57	1	0.12	0.42	7
BSF2	1.7	20.0	1.57	1	0.12	0.38	4
BSF3	5	20.0	1.57	1	0.12	0.38	11
BSF4	1.2	20.0	1.57	1	0.12	0.38	3
BSF5	12.4	17.3	1.57	1	0.12	0.33	28
BSF6	2.4	17.3	1.57	1	0.12	0.33	5
BSF7	1	14.1	1.57	1	0.12	0.27	2

Estimates of the barotropic forcing parameters, β and γ, are obtained from field data of flow and water levels. Using water level observations from gauging stations in Lake Ontario from the 1970s and simulated flow data, Hamblin (1982) performed spectrum analysis and identified several modes of barotropic oscillations. The time periods of these oscillations range from $T = 1.0$ hours to $T = 12.4$ hours, as listed in Table 4.3.1.

The corresponding amplitudes, u_o, of the oscillating barotropic flow are also listed in Table 4.3.1. u_o is obtained as follows. For each mode, the spectrum is expressed as u_o^2 in cm^2/s^2, distributed over frequency (given in Lawrence et al., 2004). By getting the square root of spectrum, we found u_o in cm/s. The analysis was based observations collected in the 1970s. Tedford (1999) analyzed more recent field observations and obtained much smaller amplitudes for the same modes. In this study, we use the average of the amplitudes given in Lawrence et al. (2004) and Tedford (1999). The resultant amplitudes are in the range of $u_o = 14.1$ to $u_o = 22.4$ cm/s (Table 4.3.2), which provide input for estimating β using equation (3.5.4).

In a simulation run, time series of the barotropic flow velocity is reconstructed from the time period and corresponding amplitude of an oscillation mode, using equation (3.6.2b). Time series for each of the modes are shown in Figure 4.1.

The other input required for estimating β [equation (3.5.4)] is the velocity scale of density-driven flow, given by $(g'Y)^{0.5}$. Based on the summer 1996 measurements (Lawrence et al., 2004), we take water temperatures as 8°C and 20°C on the lake and harbour sides, respectively, of the canal. The difference between the corresponding densities as a function of temperature (Table III of Millero 2000) is estimated to be $\rho_2 - \rho_1 \approx 2.7$ kg/m^3. Thus, $g' = 0.0265\,\text{m/s}^2$, and $(g'Y)^{0.5} = 0.53$ m/s. Estimates of β range from 0.27 to 0.42. The barotropic forcing is weak relative to the velocity scale of the density-driven flow.

The time scale for interfacial waves to travel through the canal is 0.435 hours. We assume that the density-driven flow velocity is of the same scale as interfacial wave propagations. Estimates of the barotropic forcing period parameter, γ, are obtained from equation (3.5.5). The slowest mode, with a time period of T = 12.4 hours, of the barotropic forcing has a γ value of about 28, whereas the fastest mode has a γ value of about 2. Estimates of all the friction and barotropic forcing parameters are summarised in Table 4.3.1.

4.3.2 Moderate friction simulations ($10^{-1} < \alpha < 10^{0}$)

Simulation runs for moderate friction condition use parameter values listed in Table 4.3.2. According to Lawrence et al. (2004) and Gu and Lawrence (2005), the interfacial friction coefficient is f_i = 0.004, giving r_i = 1 [equation (3.5.6)]. We assume that the sidewall friction coefficient is the same as the bottom friction coefficient, i.e. f_w = 0.0039, and therefore the sidewall friction parameter is r_w = 0.12 [equation (3.5.7)]. No surface friction is present in these runs.

Table 4.3.2: Parameter values for runs BMF1–BMF7. There is no surface friction in all the runs. Barotropic forcing in runs BMF1–BMF7 corresponds to the average of the oscillation modes described in Hamblin (1982) and Tedford (1999).

Run	T (hr)	u_o (cm/s)	α	r_i	r_w	β	γ
BMF1	3.2	22.4	0.30	1	0.12	0.42	7
BMF2	1.7	20.0	0.30	1	0.12	0.38	4
BMF3	5	20.0	0.30	1	0.12	0.38	11
BMF4	1.2	20.0	0.30	1	0.12	0.38	3
BMF5	12.4	17.3	0.30	1	0.12	0.33	28
BMF6	2.4	17.3	0.30	1	0.12	0.33	5
BMF7	1	14.1	0.30	1	0.12	0.27	2

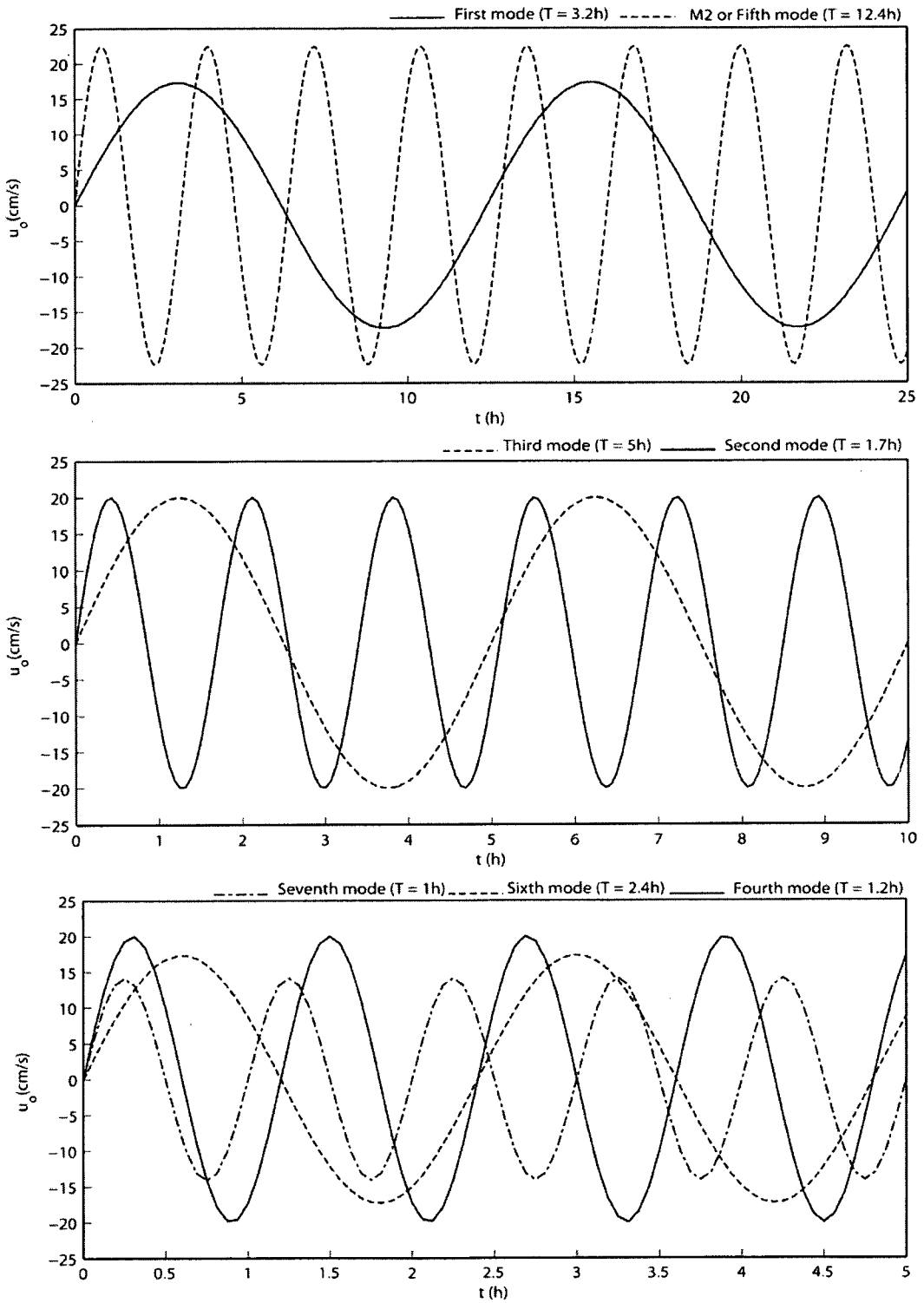

Figure 4.1: Time series of barotropic forcing for the modes listed in Table 4.3.1. The barotropic forcing parameters are the same as the strong friction simulations listed in Table 4.3.1.

4.3.3 Weak friction simulations ($a < 10^{-1}$)

For weak friction simulations (BWF1–BWF7), we simply reduce the bottom friction parameter from $\alpha = 0.30$ for the moderate simulations by an order of magnitude. That is to say that $\alpha = 0.03$ for simulations BWF1–BWF7. All other parameters are the same as for moderate friction simulations (see Table 4.3.3).

The barotropic forcing parameters are the same as the strong friction simulations listed in Table 4.3.1 and the moderate friction simulations listed in Table 4.3.2.

Table 4.3.3: Parameter values for runs BWF1–BWF7. There is no surface friction in all the runs. Barotropic forcing in runs BWF1–BWF7 corresponds to the average of the oscillation modes described in Hamblin (1982) and Tedford (1999).

Run	T (hr)	u_o (cm/s)	α	r_i	r_w	β	γ
BWF1	3.2	22.4	0.03	1	0.12	0.42	7
BWF2	1.7	20.0	0.03	1	0.12	0.38	4
BWF3	5	20.0	0.03	1	0.12	0.38	11
BWF4	1.2	20.0	0.03	1	0.12	0.38	3
BWF5	12.4	17.3	0.03	1	0.12	0.33	28
BWF6	2.4	17.3	0.03	1	0.12	0.33	5
BWF7	1	14.1	0.03	1	0.12	0.27	2

Chapter Five: Results

In this chapter we present the model results for simulation runs whose conditions are described in Chapter Four. The presentations follow the sequence of the sensitivity test runs, the steady laboratory channel runs and the Burlington Ship Canal runs. Between-run comparisons will be made where it is pertinent and possible.

5.1 Sensitivity test

All sensitivity test runs commence from the condition of lock exchange and proceed until a state of equilibrium is reached. We define the state of equilibrium as the condition of changes to dimensionless layer velocities and interface height being smaller than 10^{-6} between two successive output time steps. The equilibrium solutions of interface height above the channel bottom and layer velocities for the test runs are extracted from the model results. Note that the density-induced pressure gradient in the horizontal, which drives steady exchange flow, is dominantly associated with along-channel variations in interface height.

5.1.1 Steady exchange under strong friction

The interface heights above the channel bottom for strong friction runs SS1–SS3 (Table 4.1.1) are compared in Fig. 5.1.1. The canal portion of the model channel is between x/L = 0.5 and x/L = -0.5 (Figure 3.1). The interface profile for run SS1 is steeper relative to those for runs SS2 and SS3. This means that run SS1 predicts a larger pressure gradient in the horizontal. The predicted volume flux is lower for SS1 than for SS2 and SS3. At this point, it is not clear if the artificial open boundaries placed at $x/L = \pm 1$ (Table 4.1.1) in run SS1 have significantly affected the predictions.

The interface heights for runs SS2 and SS3 are close to each other, mainly for the canal portion of the model channel. For these two runs, the dimensionless interface heights above the channel bottom are y_2^* = 0.332 at the western end of the canal, i.e. at x/L = -0.5, y_2^* = 0.513 at the midpoint of the canal, i.e. at x/L = 0, and y_2^* = 0.698 at the eastern end of the canal, i.e. at x/L = 0.5 (Table 5.1.1). We consider that it is appropriate to place the open boundaries at $x/L = \pm 2$, with arguments that follow.

If the open boundaries are chosen to be as outwards as at $x/L = \pm 2$, solutions of interface height and hence layer velocities to the model equations will not depend on selections of open boundary locations. Such selections are completely artificial. Solutions that depend on the artificial selections are not physical. Runs SS2 and SS3 produce

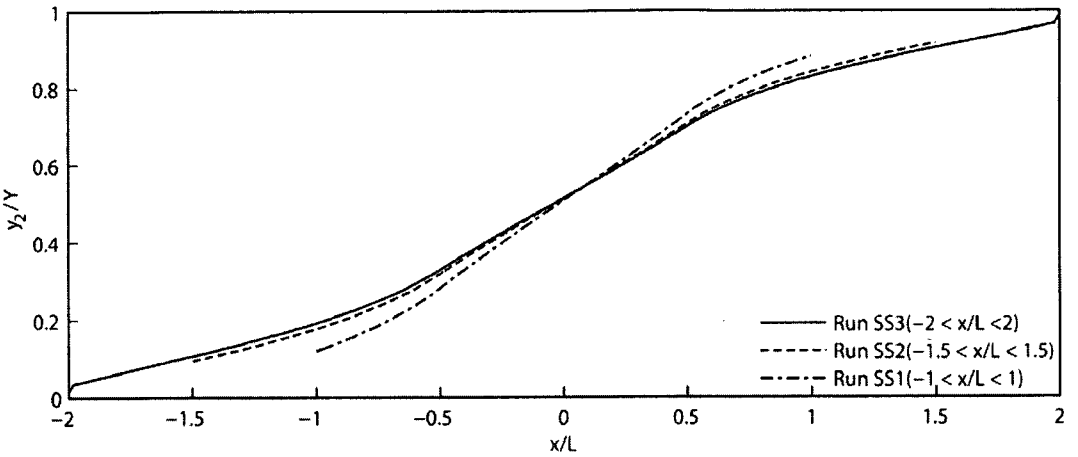

Figure 5.1: Dimensionless interface heights varying with dimensionless along-channel distance for sensitivity runs SS1, SS2 and SS3. Friction is strong ($\alpha = 1.57$; $r_i = 1$; $r_w = 0.12$).

Table 5.1.1: Changes of dimensionless interface height (y_2^*) and volume flux (q^*) as a result of r_i reduced from 1 to 0.5 in SS3.Dimensional interface height can be obtained by multiplying y_2^* by Y (= 10.6 m). Dimensional volume flux can be obtained by multiplying q^* by $\left(g'Y^3\right)^{0.5}$ (=5.618 m^3/s).

Interfacial friction	Interface height above canal bottom			Per-unit-width volume flux
	at x/L = -0.5	at x/L=0	at x/L=0.5	
r_i = 1.0	0.313	0.508	0.684	0.067
r_i = 0.5	0.328	0.513	0.698	0.090

essentially the same solutions, so we interpret that the open boundaries located at $x/L = \pm 2$ are far enough from the canal ends.

Runs SS2 and SS3 produce about the same volume flux. The dimensionless volume flux per unit width of canal is q_2 = 0.067, flowing from right to left (Fig.3.1.1). This

prediction is for $r_i = 1$. Since the exchange flow is expected to be sensitive to r_i and there are uncertainties in estimates of r_i, we rerun simulation SS3, with r_i reduced from 1 to 0.5. The effects of a reduced r_i are shown in Table 5.1.1. A decrease of interfacial friction from $r_i = 1$ to $r_i = 0.5$ causes two changes: 1) the volume flux is increased by 34%, and 2) the interface height above the canal bottom is raised.

5.1.2 Steady exchange under moderate friction

The interface heights for runs SM1–SM3 (Table 4.1.1) are shown in Figure 5.2. The friction is moderate, relative to that in runs SS1–SS3 described in the preceding section. The interface for run SM1 is steeper relative to those for runs SM2 and SM3, which is similar to the case of strong friction. The interface heights for runs SM2 and SM3 overlap. For these two runs, the dimensionless interface heights above the channel bottom are $y_2^* = 0.303$ at the western end of the canal, $y_2^* = 0.506$ at the midpoint of the canal, and $y_2^* = 0.709$ at the eastern end of the canal (Table 5.1.2).

The overlapping of the solutions for runs SM2 and SM3 supports the argument with respect to selections of open boundary locations, as presented in the preceding section. In other words, the selection of open boundaries at $x/L = \pm 2$ is suitable.

In addition to the feature of overlapping interface heights, runs SM2 and SM3 produce the same volume flux, the dimensionless volume flux per unit width of canal being

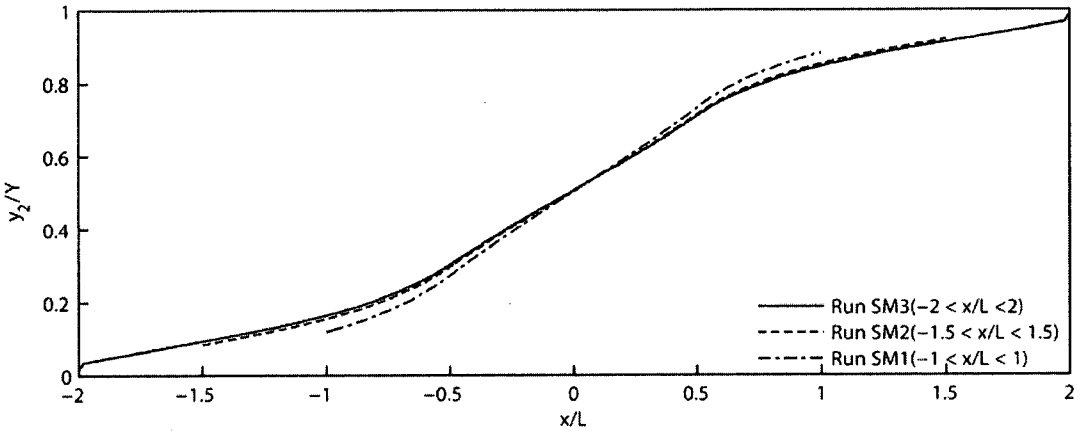

Figure 5.2: Dimensionless interface heights varying with dimensionless along-channel distance for simulation runs SM1, SM2 and SM3. Friction is moderate ($\alpha = 0.30$; $r_i = 1$; $r_w = 0.12$).

Table 5.1.2: Changes of dimensionless interface height (y_2^*) and volume flux (q^*) as a result of r_i reduced from 1 to 0.5 in SM3.Dimensional interface height can be obtained by multiplying y_2^* by Y (= 10.6 m). Dimensional volume flux can be obtained by multiplying q^* by $\left(g'Y^3\right)^{0.5}$ (=5.618 m3/s).

Interfacial friction	Interface height above canal bottom			Per-unit-width volume flux
	at x/L = -0.5	at x/L=0	at x/L=0.5	
$r_i = 1.0$	0.303	0.506	0.709	0.128
$r_i = 0.5$	0.298	0.507	0.717	0.145

$q_2 = 0.128$ (Table 5.1.2). To test the effect of interfacial friction on exchange, run SM3 is redone, with interfacial friction reduced from $r_i = 1$ to $r_i = 0.5$. The results corresponding to the two different r_i values are compared in Table 5.1.2. In terms of interface, aside from a slight increase in interface height at the eastern end ($x/L = 0.5$) of the canal, there are no significant changes. As expected, the volume flux increases when the interfacial friction factor decreases from $r_i = 1$ to $r_i = 0.5$.

5.1.3 Steady exchange under weak friction

Weak friction runs SW1–SW3 (Table 4.1.1) produce interface height (Figure 5.3) and volume flux with the same characteristics as moderate friction runs SM1–SM3 that were described in Section 5.1.2. The interface profile for run SW1 is relatively steep, and the interface heights for runs SW2 and SW3 are indistinguishable. In Table 5.1.3 we show the dimensionless interface heights above the channel bottom, together with a comparison of the dimensionless volume fluxes related to $r_i = 1$ and $r_i = 0.5$.

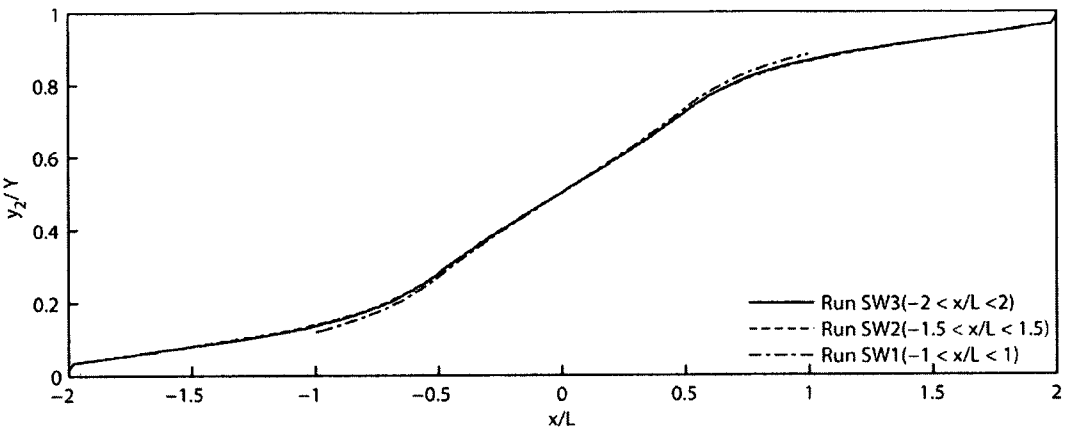

Figure 5.3: Dimensionless interface heights varying with dimensionless along-channel distance for simulation runs SW1, SW2 and SW3. Friction is moderate (α = 0.03 ; r_i = 1; r_w = 0.12).

Table 5.1.3: Changes of dimensionless interface height (y_2^*) and volume flux (q^*) as a result of r_i reduced from 1 to 0.5 in SW3. Dimensional interface height can be obtained by multiplying y_2^* by Y (= 10.6 m). Dimensional volume flux can be obtained by multiplying q^* by $\left(g'Y^3\right)^{0.5}$ (=5.618 m^3/s).

Interfacial friction	Interface height above canal bottom			Per-unit-width exchange flux
	at x/L = -0.5	at x/L=0	at x/L=0.5	
r_i = 1.0	0.280	0.501	0.722	0.177
r_i = 0.5	0.279	0.501	0.722	0.180

5.2 Comparison of model results with laboratory channel experiments

This section shows comparisons of interface height and exchange flux between the model and laboratory experiments of exchange flow.

5.2.1 5.2.1 Interface heights

Gu and Lawrence (2005) presented experimental data of interface height above the channel bottom from eight laboratory experiments of exchange flow. A snapshot of the experiments is shown in Figure 5.4, where an upper layer of lighter water flows towards the right, whereas a lower layer of density water flows towards the left. For visualization, fluorescent water-tracer dye was added to the water tank on the right hand side, which held denser water. The red box marks the canal portion of the experiment setup. A known amount of salt was added to the water tank on the right hand side in order to create a density difference between the two ends of the laboratory channel.

The eight experiments used different amounts of salt, and therefore the reduced gravity had different value from experiment to experiment. During each of the experiments, steady exchange flow through the canal was observed, which lasted a short period of time (a few minutes). From the same experiments, Gu and Lawrence (2005)

obtained fluid velocities, from which bottom friction parameter values (Table 4.2.1) and volume fluxes were derived.

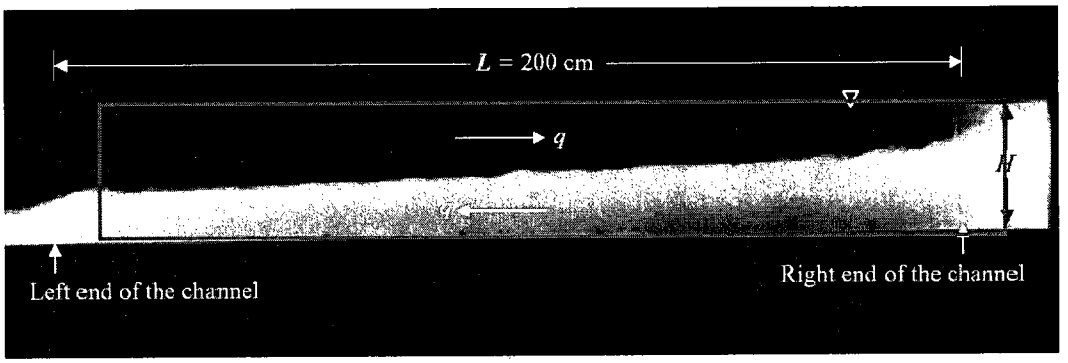

Figure 5.4: A snapshot of exchange flow experiments (from Gu and Lawrence 2005), showing oppositely flowing superimposed fluids of different density. The density interface shows small-scale wavy features due to velocity shear instability which results in turbulent motion in the vicinity of the interface.

Interface heights were measured above the channel bottom at 21 evenly spaced locations over the length of the channel. They are plotted as whiskers in Figure 5.5. These whiskers mark the lower and upper limits of the interface height from the eight experiments. The measured interface heights appear to have the least variations around the midpoint of the channel. The variations increase outwards from the midpoint, being the largest at the two ends.

For direct comparison, the predicted interface heights at equilibrium are shown as a function of distance along the channel in Figure 5.5 the predicted interface heights above the channel bottom are plotted more or less through the middle of the whiskers. This is

very encouraging. For all the simulation runs (LC1–LC16), the predicted interface heights have the smallest variations around the midpoint of the channel, and increasing variations toward the channel's ends. This feature of the model results matches the observation from the laboratory experiments.

A close examination of the predicted interface heights reveals a number of interesting characteristics. First, within the group of runs LC1–LC8 (Table 4.2.1), the predicted interface heights for run LC8 have the most gradual variations over the length of the channel. This run has the lowest friction parameter (α and r_w) values. Thus, we may conclude that exchange flow with lower friction exhibits a less steep interface profile. For this reason, the interface profile is the steepest for run LC1, as friction is the highest among the eight runs (Table 4.2.1). The interface profiles for runs LC2 – LC7 (not shown) are between those for runs LC1 an LC8. Some of the interface profiles are indistinguishable because all friction is on the same order of magnitude, being weak with $\alpha < 0.1$.

Secondly, the group of runs LC9–LC16 uses higher friction than the group of runs LC1–LC8. The interface profile for run LC9 is the steepest, and the interface profile for runs LC16 is plotted between for runs LC1 an LC8. The interface profiles for runs LC10 – LC15 (not shown) are plotted between those for runs LC9 and LC16.

Thirdly, all interface profiles (Figure 5.5) show non-linear variations over the length of the channel. For LC9 which produce the steepest profile, the interface heights are

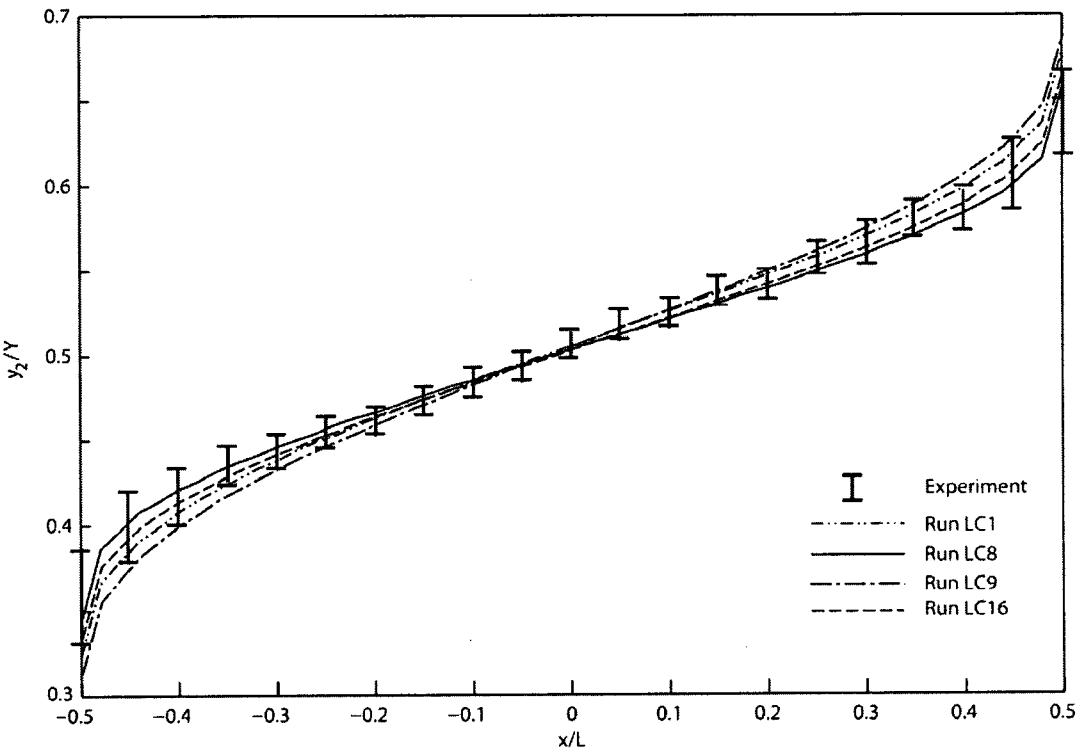

Figure 5.5: A comparison between predicted and measured interface heights, varying over the length of the channel the experimental data combined the measurements from the eight experiments described in Gu and Laurence (2005).

approximately equal to $0.5Y$ above the channel bottom at the midpoint of the channel, $0.34Y$ at the left end of the channel (x = -$0.5L$), and $0.34Y$ from the water surface at the right end of the channel (x = $0.5L$). This means an insignificant asymmetry, although there is a difference in friction between the channel bottom and the water surface. Friction is present on the channel bottom, but is absent at the surface.

5.2.2 Exchange flux

The predicted exchnage fluxes are in excellent agreement with the experimenal data (Figure 5.6). The predicted exchange fluxes are obtained by extracting interface height y_2^* and lower layer velocity u_2^* of the lower layer at the midpoint of the channel and then multiplying y_2^* by u_2^*. The dimensional exchange fluxes are calculated as $y_2^* u_2^* \sqrt{g'YYB}$. The volune fluxes (squares) for runs LC9–LC16 are plotted below those for run LC1-LC8, meaning that an increase in sidewall friction from $r_w = 0.92$ for runs LC1–LC8 to $r_w = 1.84$ for runs LC9–LC16 has reduced volume fluxes. However, the reduction between each pairs of correodponing runs (e.g. LC1 vs. LC9, see Table 4.2.1) is not so large. This is because the overall frition that is controlled by the α value [eqution (3.5.2)] does not have a large difference.

The differnces in volume flux between the different simulation runs or between the different experiments (Figure 5.6) are associated with different values for the reduced gravity. We show the values of the reduced gravity and corresponding volume fluxes in Table 5.2.1. The volume flux is proportional to $\sqrt{g'}$. Experimental volume fluxes increases from 217 cm^3/s at $\sqrt{g'} = 0.27$ $cm^{1/2}/s$ to 599 cm^3/s at $\sqrt{g'} = 1.83$ $cm^{1/2}/s$. The corresponding density-driven velocity scales are 2.7 and 7.2 cm/s, and that the corresponding volume fluxes for the model runs are 230 and 645 cm^3/s. Thus, the

comparisons between (217 vs. 230 cm^3/s, 599 vs. 645 cm^3/s) the model and the experiments are excellent.

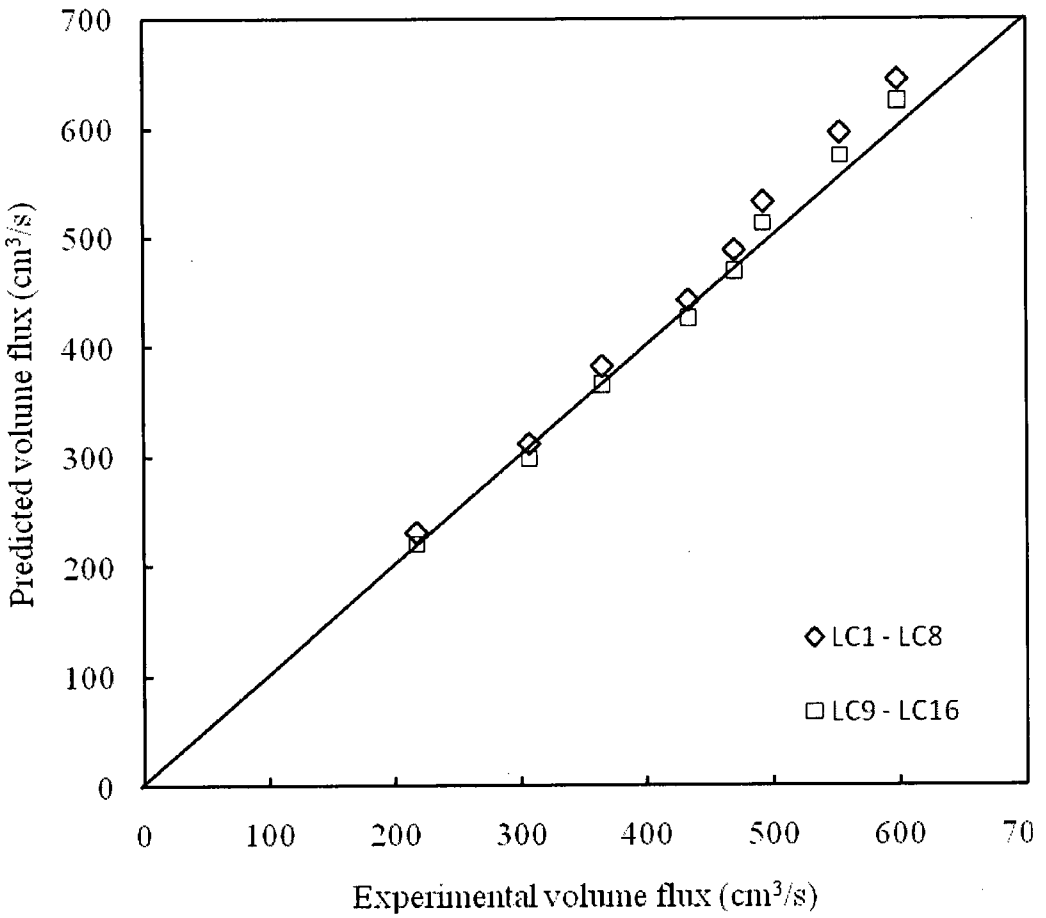

Figure 5.6: A comparison of volume fluxes between the model and experiments. The experimental data are from Gu and Lawrence (2005).

Table 5.2.1: Comparison of volume fluxes (Q) between the experiments (Gu and Lawrence, 2005) and model runs LC1–LC8. The run parameters are listed in Table 4.2.1.

Run	g'	$(g'Y)^{0.5}$	Q		
	(cm/s^2)	(cm/s)	Experiment (cm^3/s)	Model (cm^3/s)	Relative error (%)
LC1	0.27	2.7	217	230	5.8
LC2	0.49	3.7	307	311	1.4
LC3	0.72	4.5	365	382	4.8
LC4	0.95	5.2	433	443	2.2
LC5	1.14	5.6	470	488	4.0
LC6	1.33	6.1	492	533	8.2
LC7	1.61	6.7	553	596	7.8
LC8	1.83	7.2	599	645	7.7

The exclusion of sidewall friction will produce unrealistic results. This is proved by conducting eight model runs with r_w= 0. The predicted volume fluxes for these runs are higher than the model results for corresponding runs presented in Table 5.2.1 (r_w = 0.92) and Table 5.2.2 (r_w = 1.84). For example, with r_w = 0 and other conditions identical to LC1, the volume flux is 242 cm^3/s. Also, with r_w = 0 and other conditions identical to LC8, the volume flux is 663 cm^3/s. The relative errors for the runs with r_w= 0 are higher, compare to the errors presented in the two tables. Sidewall must be included for realistic prediction.

Table 5.2.2 : Comparison of volume fluxes (Q) between the experiments (Gu and Lawrence, 2005) and model runs LC9–LC16. The run parameters are listed in Table 4.2.1.

Run	g'	$(g'Y)^{0.5}$	Q		
	(cm/s^2)	(cm/s)	Experiment (cm^3/s)	Model (cm^3/s)	Relative error (%)
LC9	0.27	2.7	217	220	1.1
LC10	0.49	3.7	307	298	-3.0
LC11	0.72	4.5	365	366	0.3
LC12	0.95	5.2	433	426	-1.7
LC13	1.14	5.6	470	469	-0.1
LC14	1.33	6.1	492	513	4.2
LC15	1.61	6.7	553	575	3.9
LC16	1.83	7.2	599	625	4.4

The relative errors between the experiments and model are small, ranging from 1.4% to 8.2% (Table 5.2.1), although it appears that in runs LC1—LC8 the model has systematically over predicted the volume flux. The problem of over prediction is removed in runs LC9 to LC16; probably the sidewall friction factor of r_w = 1.84 (Table 4.2.1) more realistically reflects the experiment condition. In LC9—LC16, the relative errors between the experiments and model are small, ranging from 1.1% to 4.4%, and there is no systematic under-prediction or over-prediction by the model.

5.3 Exchange through the Burlington Ship Canal

All the Burlington Ship Canal runs (see Tables 4.3.1, 4.3.2, and 4.3.3) use the model channel between x = -2 and x = 2 (Figure 3.1). Time-dependent barotropic forcing in the form of equation (3.6.2) is present in these runs, and so is friction. Each of the runs covers more than ten cycles of barotropic forcing. Solutions of interface heights and layer velocities produced by the runs are time dependent.

In this section we extract the interface heights and layer velocities at the midpoint (x/L = 0) of the canal from the model results for the last three cycles of barotropic forcing, and present them as time series. Also, time series of volume fluxes are derived from the extracted interface heights and layer velocities. These time series are presented. The solutions at the midpoint of the canal are representative. At other locations along the canal, model solutions have similar characteristics.

5.3.1 Exchange under strong friction

Simulation runs BSF1–BSF7 have strong friction. Time series of the interface heights at x/L = 0 for these runs are shown in Figure 5.7 and Figure 5.8. It is a common feature that the interface heights fluctuate in a periodic manner. This is an expected response to the periodic barotropic forcing. The extent of the up-and-down movement of the interface

depends on the magnitude of the barotropic forcing.

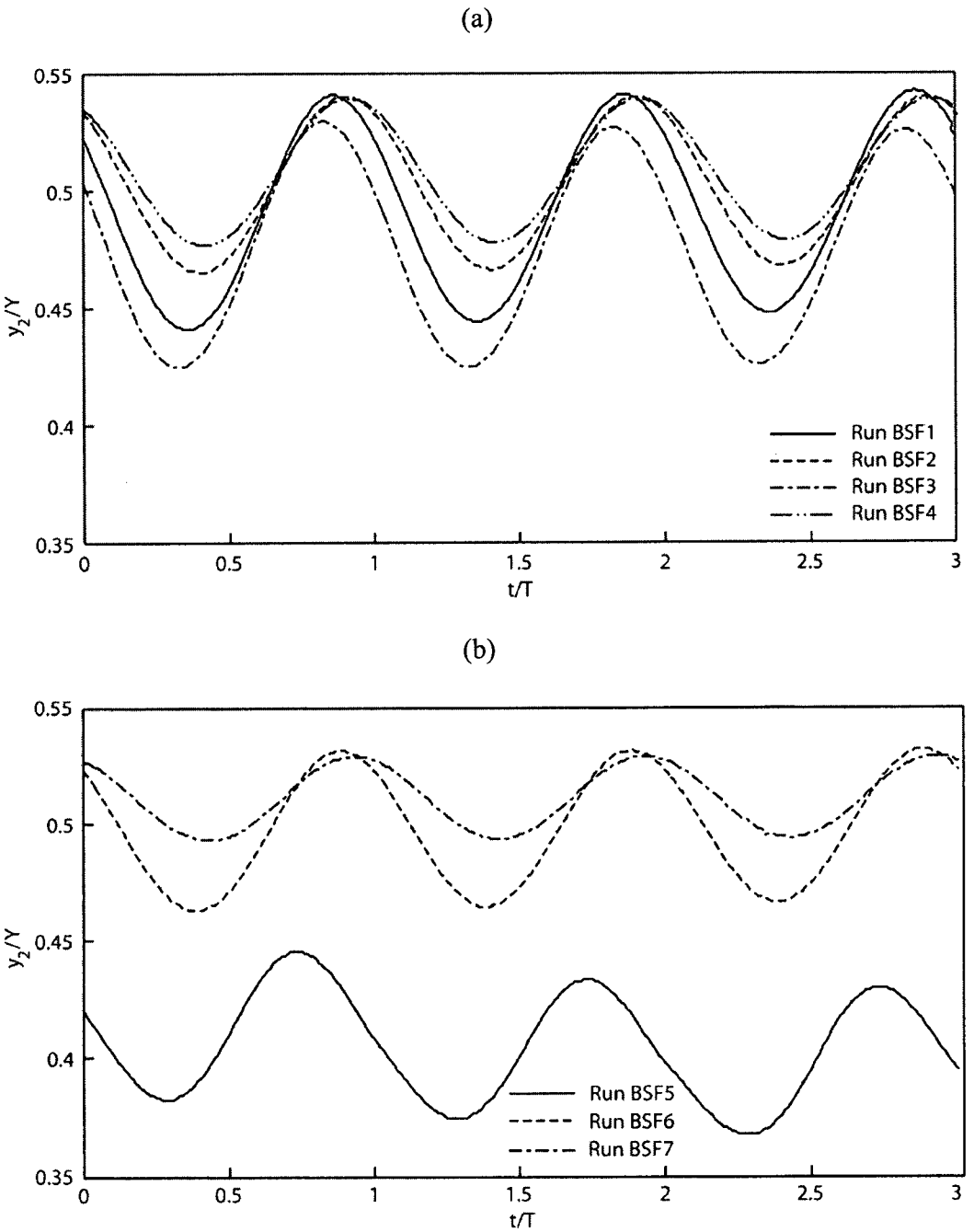

Figure 5.7: Time series of dimensionless interface heights at x/L = 0: (a) for runs BSF1–BSF4, and (b) for runs BSF5–BSF7. Dimensional interface heights can be obtained by multiplying y_2^* by Y (= 10.6 m).

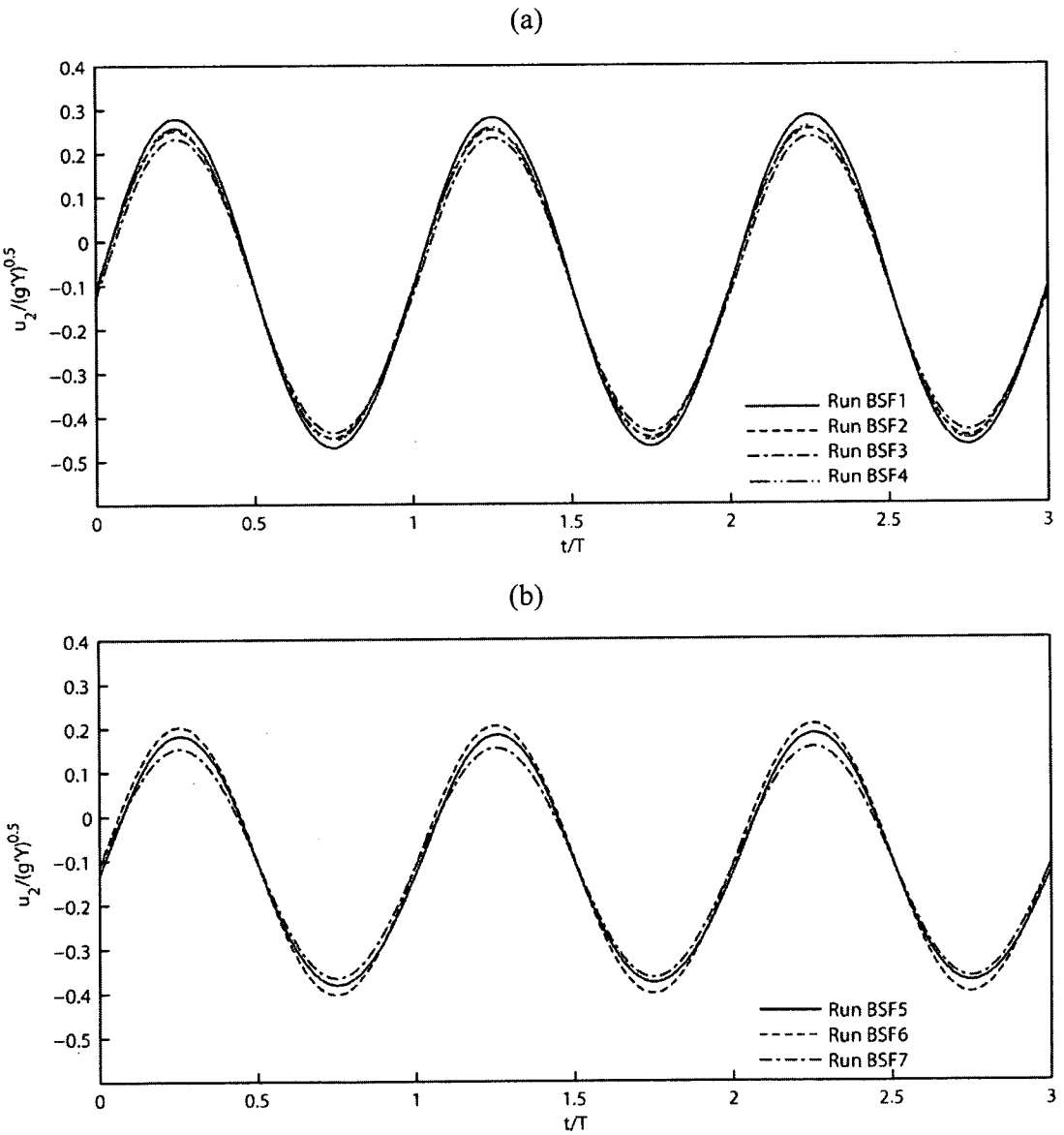

Figure 5.8: Time series of dimensionless lower-layer velocity at x/L = 0: (a) for runs BSF1–BSF4, and (b) for runs BSF5–BSF7. Over a barotropic-forcing cycle, the lower layer flows from Lake Ontario to Hamilton Harbour when $u_2 < 0$, and from the harbour to the lake when $u_2 > 0$. The definition of flow direction is shown in Figure 3.1b. Dimensional velocity can be obtained by multiplying u_2^* by $\sqrt{g'Y}$ (= 0.53 m/s).

For example, in BSF1 where the forcing has the largest magnitude of the seven runs (Table 4.3.1), the interface height fluctuates over time between $y_2^* = 0.482$ and $y_2^* = 0.523$ (dimensionless). This range corresponds to a dimensional distance of 0.43 m, as obtained by multiplying y_2^* by the vertical length scale of $Y = 10.6$ m. Run BSF7 produces the smallest fluctuations (0.23 m) in the vertical, as the barotropic forcing is the weakest among the seven runs.

The vertical fluctuations for the other runs range from 0.23 m to 0.43 m. It is important to note that the above-mentioned ranges of vertical fluctuations are the responses of the interface to individual barotropic forcing modes.

Similar to the interface, layer velocities exhibit periodic variations with time (Figure 5.8), in response to barotropic forcing. The amplitude of the periodic variations is proportional to the amplitude of the barotropic forcing mode. In run BSF1, the mode is the strongest (Table 4.3.1), resulting in the largest layer-velocity fluctuations.

In the first half $(0 < t/T < 0.5)$ of each forcing cycle, barotropic forcing works against the lower layer; the result is to weaken the left-to-right flow or even reverse its flow direction. In the second half $(0.5 < t/T < 1)$ of each forcing cycle, barotropic forcing works with the lower layer; the result is to enhance the left-to-right flow. To

illustrate the aforementioned points, we take run BSF1 as an example. Around $t/T = 0.25$, 1.25..., the lower-layer flow is reversed in direction by barotropic forcing, with an otherwise negative (flowing from the lake to the harbour) velocity value of $u_2^* = -0.0132$ (from run SS3) becoming a positive (flowing from the harbour to the lake) velocity value of large than 0.25.

In a similar way, one can describe the relationship between barotropic forcing and the upper-layer velocity. We emphasize that a flow reversal can take place under the action of barotropic forcing. This does take place in all the strong friction runs (BSF1–BSF7), as is seen from the positive lower-layer velocity values around $t/T = 0.25$, 1.25..., in Figure 5.8.

On the basis of predicted lower-layer velocity and interface height, we can derive the time-dependent exchange flux per unit width of canal, as

$$q_2^* = y_2^* u_2^* \tag{5.3.1}$$

Time series of the volume fluxes at $x/L = 0$ are shown in Figure 5.9.In terms of volume flux, barotropic forcing works with the lower layer in the second half ($0.5 < t/T < 1$) of each forcing cycle. The forcing increases the right-to-left flow velocity and at the same time lifts the interface above the canal bottom from its equilibrium level and hence enlarges the cross-sectional area through which the lower layer is flowing.

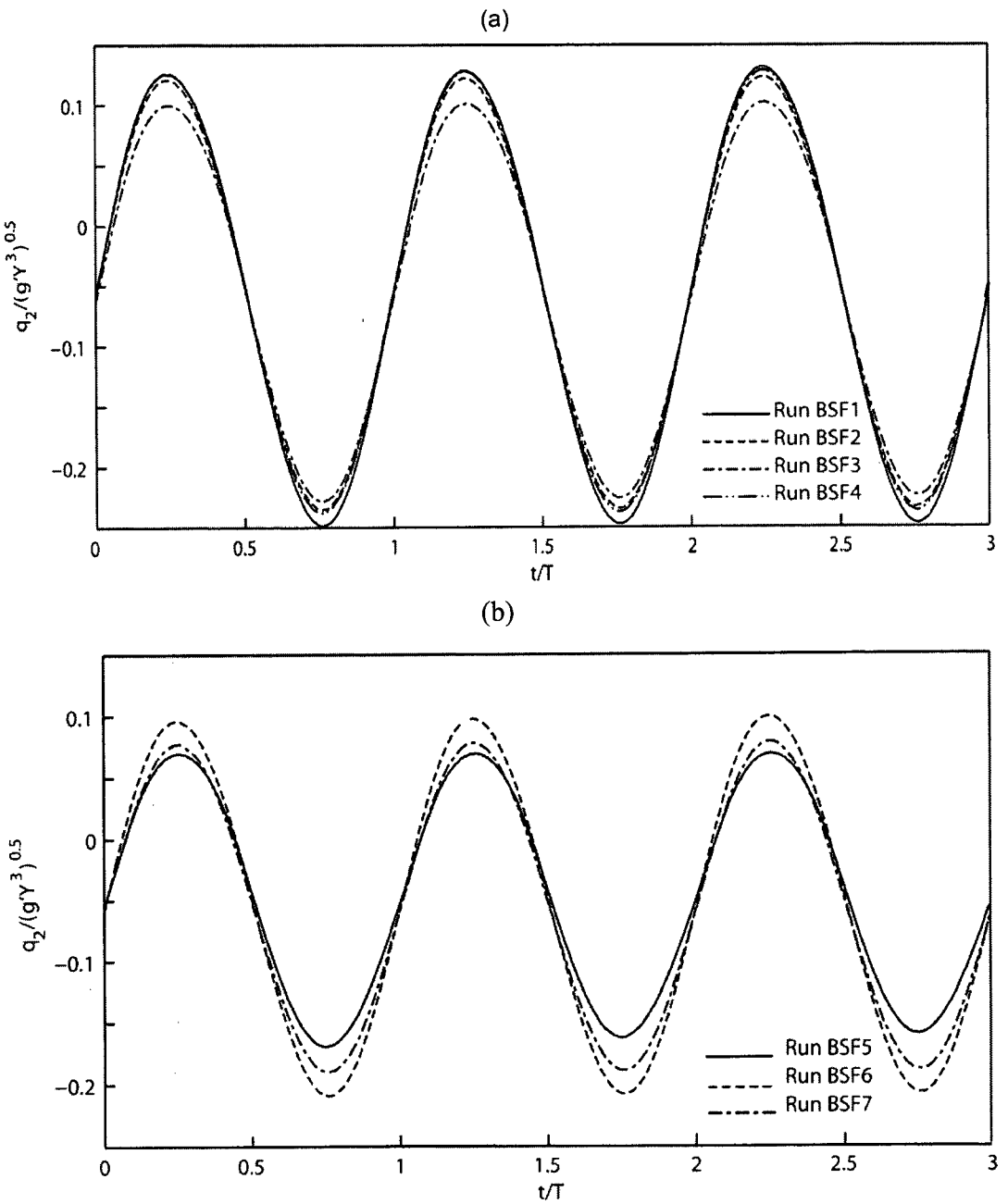

Figure 5.9: Time series of dimensionless volume flux per unit width of canal in the low layer at x/L = 0: (a) for runs BSF1 to BSF4, and (b) for runs BSF5 to BSF7. Negative values for volume flux indicate that the flow is in the direction of the negative x-axis or

from the lake to the harbour. Dimensional volume flux can be obtained by multiplying q_2^* by $\left(\sqrt{g'Y^3}\right)$ (= 5.618 m^2/s).

For time-dependent runs, it is meaningful to obtain the time average of volume fluxes over one or more time periods of barotropic forcing as

$$\bar{q}_2^* = \frac{1}{T}\int_0^T y_2^* u_2^* dt \tag{5.3.2}$$

We may further calculate time averages of dimensional volume fluxes of Lake Ontario Water into Hamilton harbour from

$$Q_2 = BY\sqrt{g'Y}\bar{q}_2^* \tag{5.3.3}$$

These time averages of volume fluxes will be discussed later in Chapter Six.

5.3.2 Exchange under moderate friction

For moderate friction runs BMF1–BMF7, the temporal variations of interface heights above the canal bottom at the midpoint (x/L = 0) of the canal are shown in Figure 5.10. The time-dependent barotropic forcing causes the interface to move up and down. For example, in run BMF1, the interface fluctuates over time between y_2^* = 0.460 and y_2^* = 0.565. The fluctuations in the vertical represent a dimensional distance of 1.11 m. Run BMF7 produces the smallest vertical fluctuations of about 0.40 m, as the barotropic forcing is the weakest among the seven runs.

The layer velocity exhibits periodic variations with time (Figure 5.11), in response to barotropic forcing. The magnitude of the variations appears to be proportional to the strength of the barotropic forcing, which is similar to the case of strong friction case. For example, in run BMF1, the forcing mode is the strongest (Table 4.3.2), resulting in the largest layer-velocity fluctuations (Fig. 5.11). It is important to note that barotropic forcing can reverse the direction of layer velocity. This is seen in Figure 5.11 where the lower layer velocity has positive values, meaning the lower layer flows from the harbour to the lake.

Barotropic forcing can arrest the otherwise flowing fluid. This is seen as the lower layer having zero velocities. This is particularly the case in run BMF7 at model time t/T = 0.25, 1.25, 2.25, ...The barotropic forcing in runs BMF1–BMF6 is stronger than that in run BFM7 (Table 4.3.2). Around model times t/T = 0.25, 1.25, 2.25, ...the lower layer velocities become positive (Figure 5.11), meaning that stronger barotropic forcing has caused the density-driven flow to reverse direction.

Barotropic forcing can accelerate the layer, meaning that the lower layer has much high velocities (u_2 = -0.6 in Figure 5.11), relative to the case of steady exchange without barotropic forcing. Again, it is important to note that these responses are to individual barotropic forcing modes.

(a)

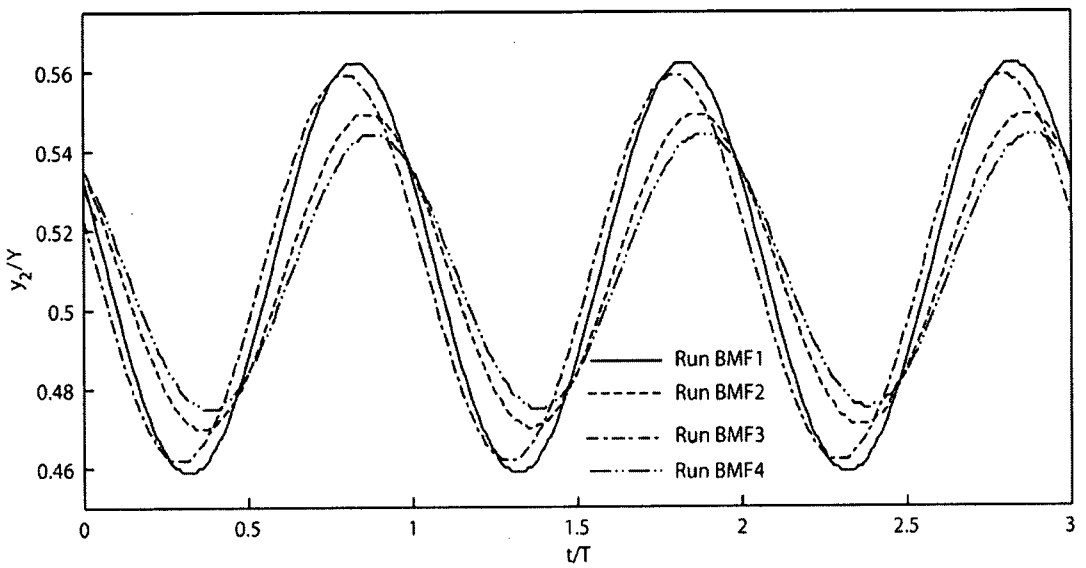

(b)

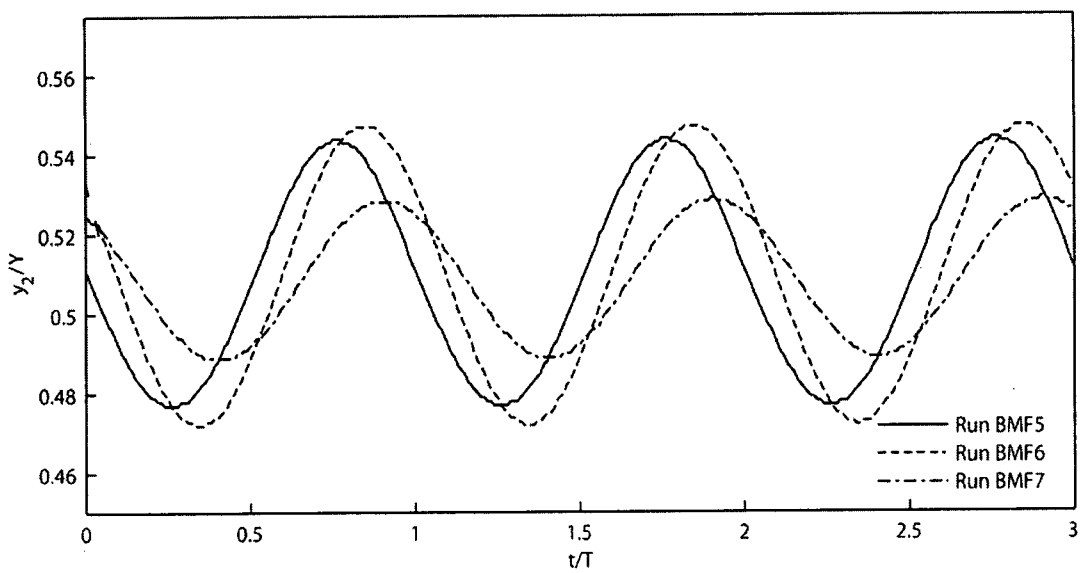

Figure 5.10: Time series of interface heights at the midpoint (x = 0) of the canal: (a) for runs BMF1–BMF4, and (b) for runs BMF5–BMF7. The interface heights are normalized by the total depth of flow. The run parameters are listed in Table 4.3.2. Dimensional interface heights can be obtained by multiplying y_2^* by Y (= 10.6 m).

(a)

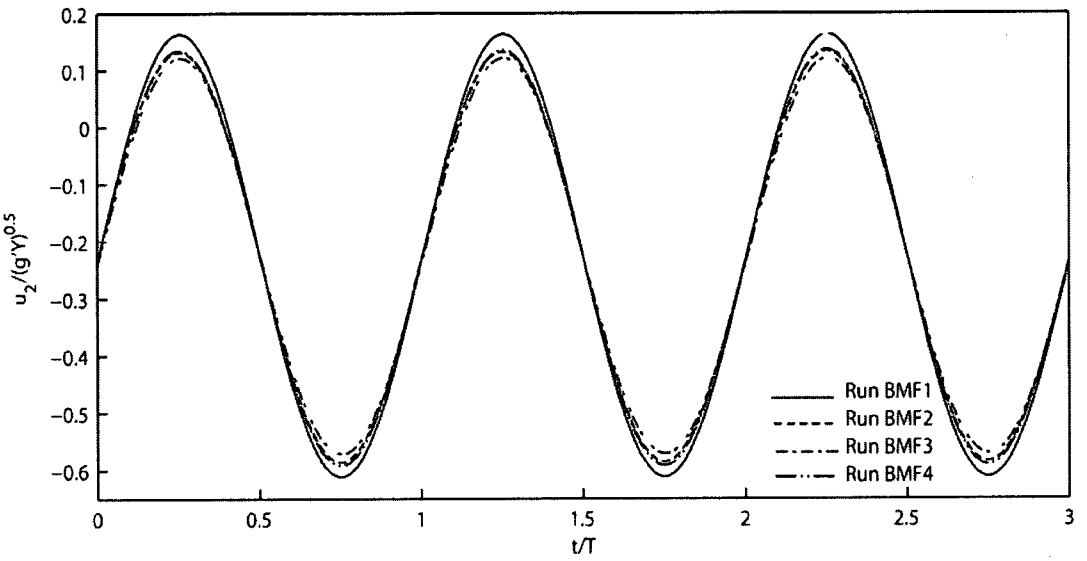

(b)

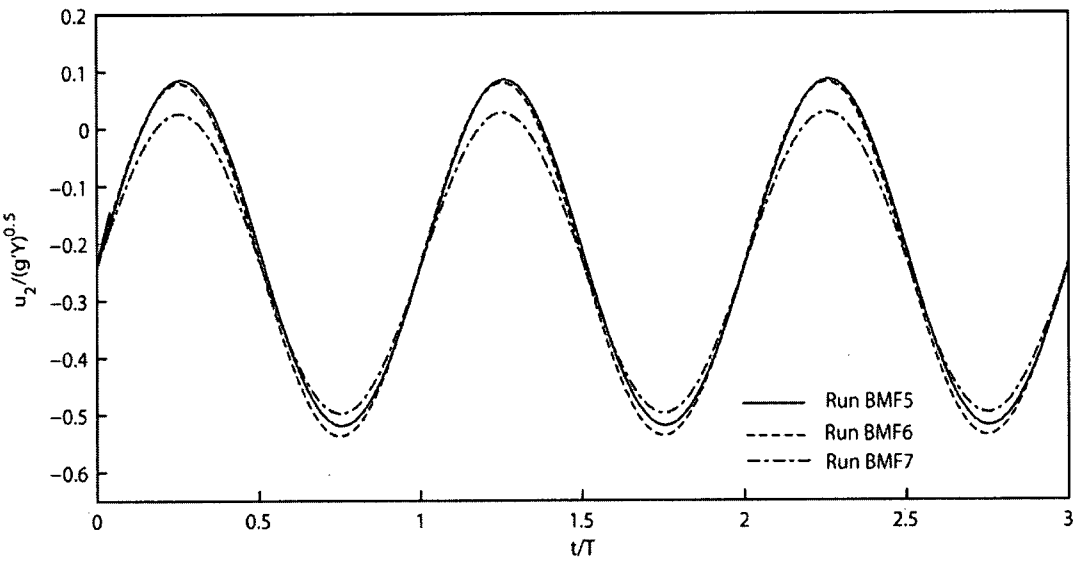

Figure 5.11: Time series of normalized lower-layer velocity at the midpoint (x = 0) of the canal: (a) for runs BMF1–BMF4, and (b) for runs BMF5–BMF7. The negative sign of the vertical axis indicates that the flow is in the direction of the negative x-axis (from right to left, see Figure 3.1b). Run parameters are listed in Table 4.3.2. Dimensional velocity can be obtained by multiplying u_2^* by $\sqrt{g'Y}$ (=0.53 m/s).

Time series of exchange fluxes at the midpoint of the canal for run BMF1–BMF7 are shown in Figure 5.12. The time series for run BMF1 shows the largest fluctuations in the vertical, whereas the time series for run BMF7 indicates the smallest fluctuations. The time series for the other runs are plotted between those for runs BMF1 and BMF7.

For the lower layer, the time average of volume fluxes is given by equation (5.3.2). Note that $\overline{q}_1 = -\overline{q}_2$. The corresponding dimensional averages of exchange flow rates can be obtained from equation (5.3.3).

(a)

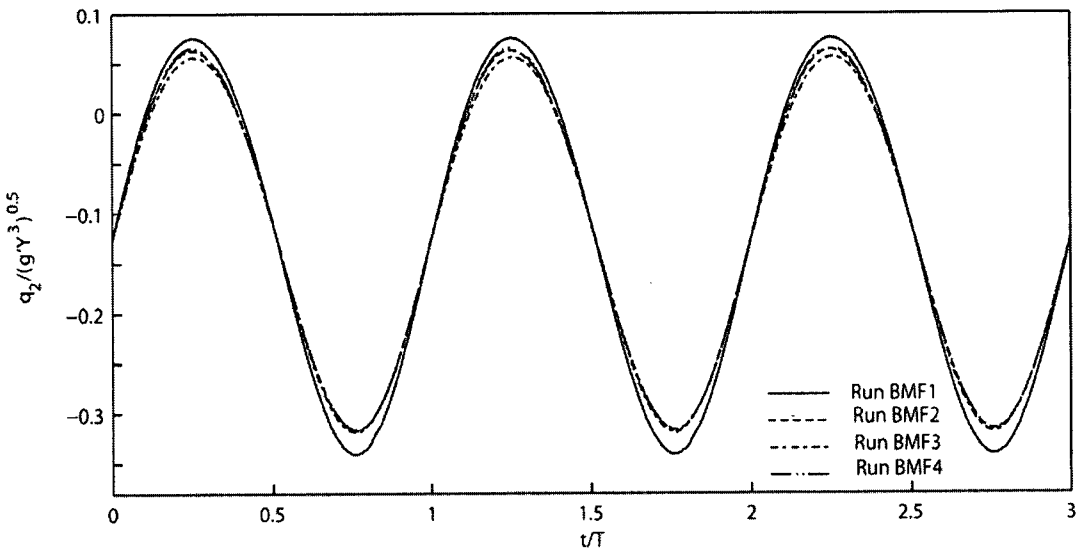

(b)

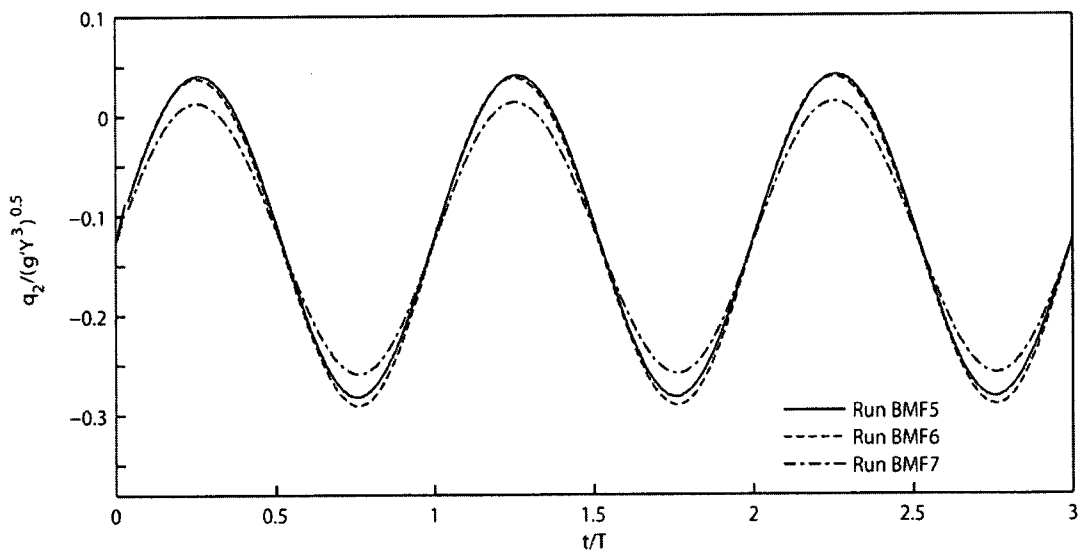

Figure 5.12: Time series of dimensionless lower-layer volume flux per unit width of canal at x/L = 0: (a) for runs BMF1 to BMF4, and (b) for runs BMF5 to BMF7. Negative values for volume flux indicate that the flow is from Lake Ontario to Hamilton Harbour. Dimensional volume flux can be obtained by multiplying q_2^* by $\left(\sqrt{g'Y^3}\right)$ (= 5.618 m^2/s).

5.3.3 Exchange under weak friction

For weak friction runs BWF1–BWF7, time series of interface heights, lower-layer velocity and volume flux are shown in Figures 5.13, 5.14 and 5.15, respectively. All the time series are extracted from the model results of the corresponding runs at the midpoint (x/L=0) of the canal. The characteristics of vertical fluctuations and temporal variations are similar to the cases of strong and moderate friction, which will not be repeated here.

The main difference from the two earlier cases is that there is no flow direction reversal, and for run BWF1, the flowing lower layer has velocities close to zero at t/T = 0.25, 1.25..., meaning that the lower layer is almost arrested by barotropic forcing. The other difference is that the vertical fluctuations are to a less extent. This is because the density-driven flow is stronger as friction decreases to the weak level, and hence barotropic forcing becomes less influential.

(a)

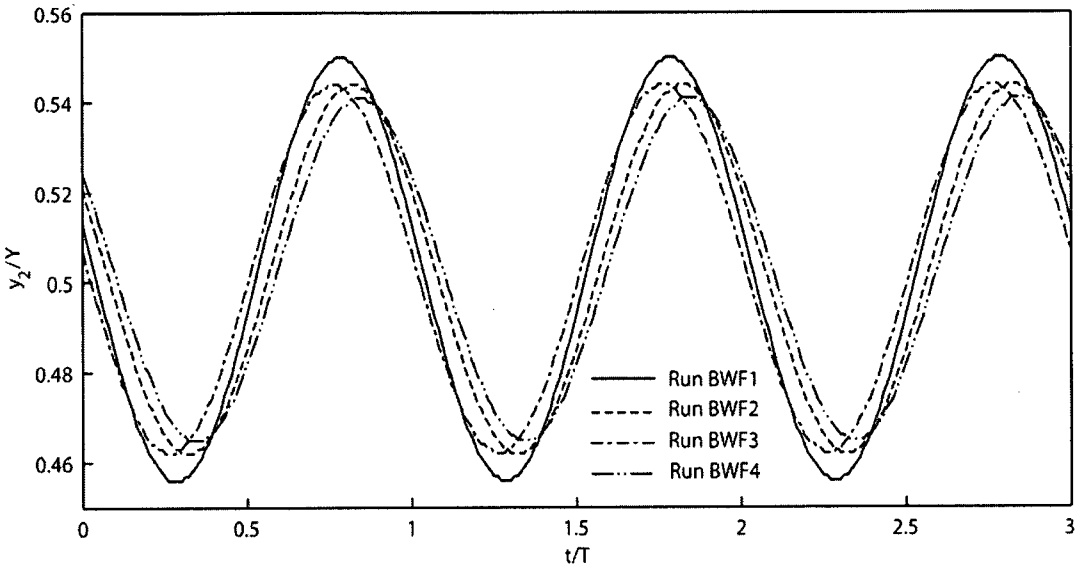

(b)

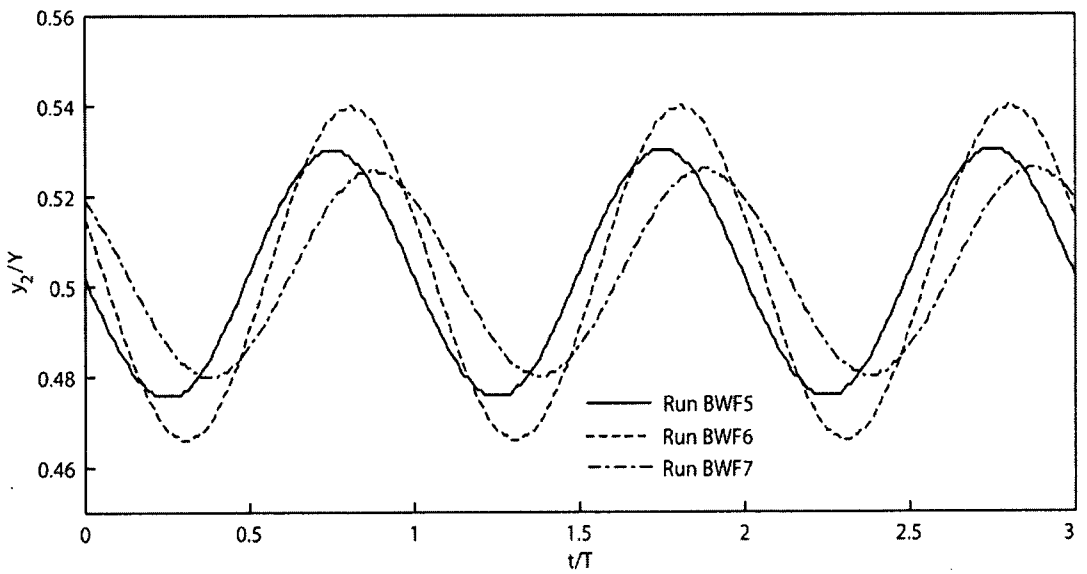

Figure 5.13: Time series of dimensionless interface height above the canal bottom at x/L = 0: (a) for runs BWF1–BWF4, and (b) for runs BWF5–BWF7. Dimensional interface heights can be obtained by multiplying y_2^* by Y (= 10.6 m).

(a)

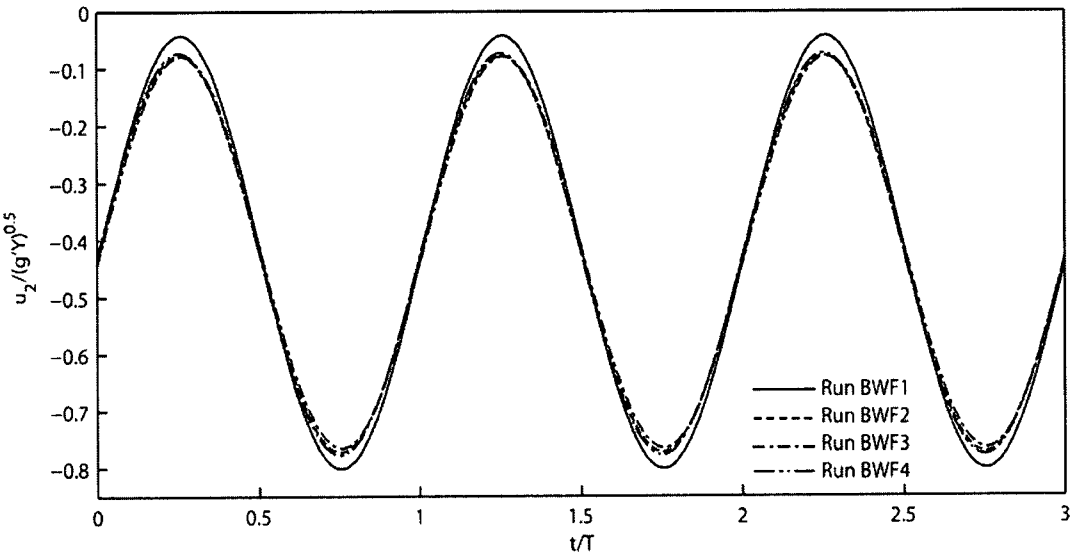

(b)

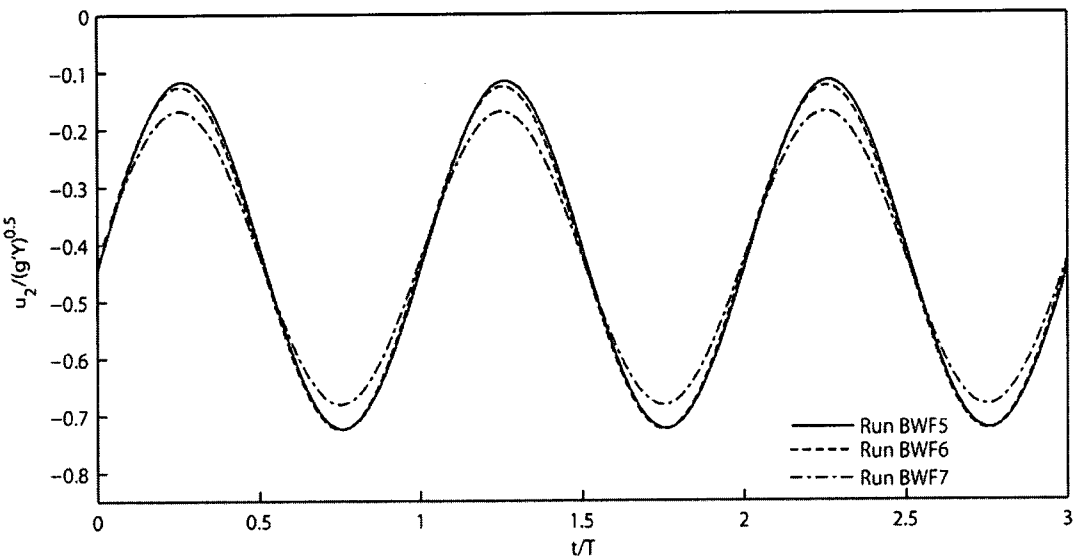

Figure 5.14: Time series of dimensionless lower-layer velocity at x/L = 0: (a) for runs BWF1–BWF4, and (b) for runs BWF5–BWF7. Dimensional velocity can be obtained by multiplying u_2^* by $\sqrt{g'Y}$ (= 0.53 m/s).

(a)

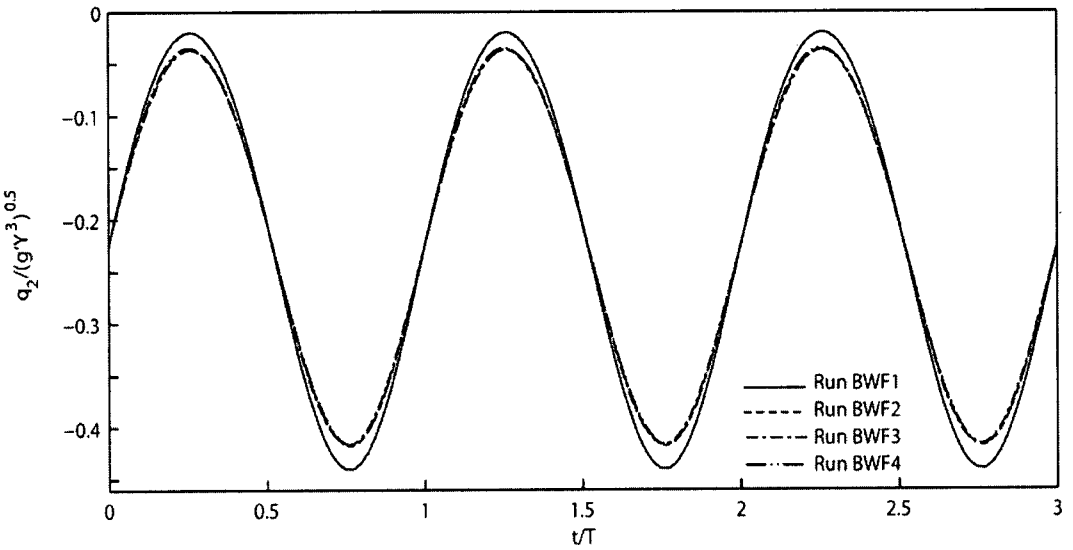

(b)

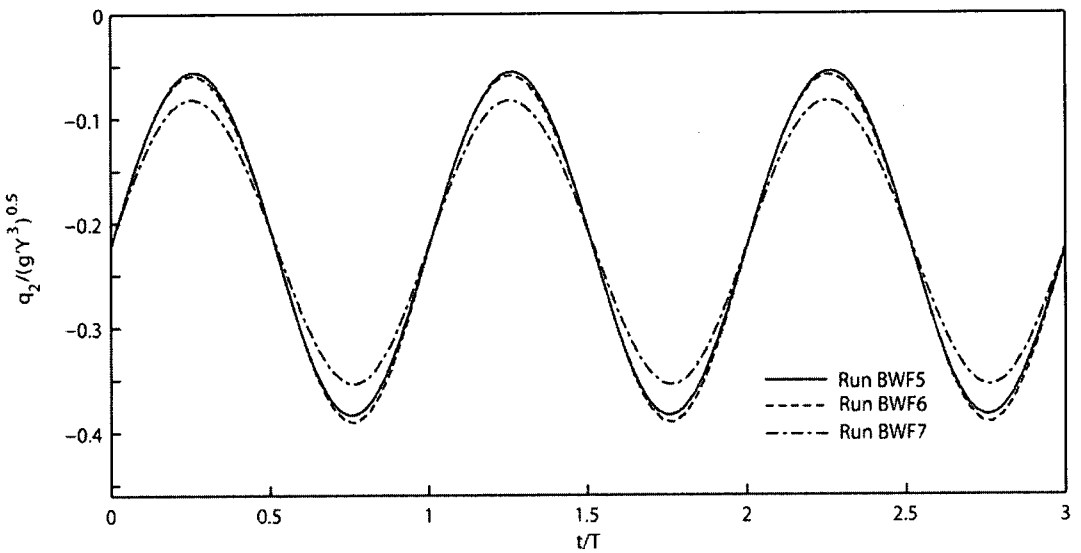

Figure 5.15: Time series of dimensionless volume flux at x/L = 0: (a) for runs BWF1–BWF4, and (b) for runs BWF5–BWF7. Dimensional volume flux can be obtained by multiplying q_2^* by $\left(\sqrt{g'Y^3}\right)$ (= 5.618 m^2/s).

Chapter Six: Discussion

In this chapter our discussion focuses on volume fluxes based on field observations, theoretical analyses and model simulations and their comparisons. We also discuss the role of barotropic forcing and friction in the determination of volume flux.

6.1 Comparisons of volume fluxes

Based on the field observations of flow from the Burlington Ship Canal for the period of 8–28 July 1996, Lawrence et al. (2004) gave the 12-hour and fifteen-minute average flows of harbour water to the lake, as

$$\overline{Q}_{12h} = 25 \text{ to } 50 \text{ (m}^3\text{/s)},$$

and $$\overline{Q}_{15\,min} = 100 \text{ (m}^3\text{/s)}$$

The fifteen-minute average flows were much higher than the 12-hour average flow. These largely different averages indicate that the exchange flow through the canal fluctuated significantly with time. Thus, it is more appropriate to compare the observed 12-hour average with predicted steady or time-average volume fluxes for simulation runs.

Theoretically, when there are no other driving forces (or both barotropic forcing and friction are ignored), density-driven two-layer exchange through a horizontal contraction

gives an inviscid volume flux in each layer (Armi and Farmer 1986; Lawrence 1990; Hogg et al. 2001), as

$$Q_{inv} = \frac{1}{4}\sqrt{g'Y^3}B \qquad (6.1.1)$$

For the exchange flow through the Burlington Ship Canal, an estimate of the reduced gravity is $g' = 0.0265\ \mathrm{m/s^2}$, the average total depth of flow is $Y = 10.6$ m, and the width of the canal is $B = 89$ m. The theoretical volume flux will be

$$Q_{inv} = 125\ \ (\mathrm{m^3/s})$$

Given that this theoretical value is for the condition of vanishing friction, it should be considered as the upper bound of steady volume flux through the canal. In other words, we expect the true volume flux to be below Q_{inv}.

In this study we calculated the volume fluxes, using equations (5.3.1), from predicted y_2 and u_2 for simulation runs SS3, SM3 and SW3 (without barotropic forcing). The volume fluxes are given in Table 6.1.1.

Table 6.1.1: Volume fluxes in each layer through the canal for steady simulation runs SS3, SM3 and SW3.

Run	Volume flux in each layer (m^3/s)	
	with $r_i = 1$	with $r_i = 0.5$
SS3	34	43
SM3	64	73
SW3	89	90

When the interfacial friction parameter is given a value of r_i = 1, the predicted volume fluxes are in the range of

$$Q_{pred} = 34 - 89 \, (\mathrm{m}^3/\mathrm{s})$$

which depends on the overall friction that is controlled by the α. Since the predicted volume fluxes appear to be sensitive to friction, we reran the model for the same conditions as SS3, SM3 and SW3, except the interfacial friction parameter was reduced from r_i = 1 to r_i = 0.5. As expected, the volume fluxes for r_i = 0.5 increase from those for r_i = 1 (Table 6.1.1).

With respect to the model results shown in Table 6.1.1, we make two observations. First, the predicted values are indeed within the theoretical upper bound of $Q_{inv} = 125$ (m^3/s). More importantly, as friction decreases from run SS3 to SW3, the predicted volume flux increases to 89 m^3/s, being closer to the upper bound. Secondly, the predicted volume flux for strong friction appears to be comparable with the observed volume flux. It is important to note that this comparison does not take into account of the barotropic forcing.

The predicted volume fluxes for simulation runs with barotropic forcing are summarized in Table 6.2.1. The volume fluxes are calculated using equations (5.3.1) and

(5.3.2) from the predictions of y_2 and u_2. All the time averages of volume fluxes shown in the table are below the upper bound of Q_{inv}. The observed $\overline{Q}_{12h}$ appears between the time averages for the strong friction runs (BSF1–BSF7) and the moderate friction runs (BMF1–BMF7).

6.2 Exchange inhibition by barotropic forcing

The effects of barotropic forcing on volume flux can be revealed by making between-run comparisons. The steady run SS3 (without barotropic forcing) and the unsteady runs BSF1–BSF7 (with weak barotropic forcing) have the same friction parameter values (Table 4.1.1 and Table 4.3.1).

Exchange inhibition by barotropic forcing also takes place at moderate friction. This is seen by comparing the volume flux (64 m^3/s shown in Table 6.1.1) for the run SM3 to those (59–62.5 m^3/s shown in Table 6.1.2) for runs unsteady runs BMF1–BMF7. However, there are only slight reductions to volume flux.

By inference, there exists a level of friction at which oscillating barotropic forcing has zero net influence on volume fluxes when averaged over one or more oscillation periods. Li and Lawrence (2009) first noted that when friction is strong, exchange can be inhibited by weak barotropic forcing. The above discussion indicates that exchange inhibition by

barotropic forcing can also take place, even if friction is moderate. In the limit of vanishing friction, Helfrich (1995) concluded that barotropic forcing always enhance exchange.

Table 6.2.1: Time-averages ($\overline{Q}$) of predicted unsteady volume fluxes for unsteady runs. The volume fluxes for steady runs SS3, SM3 and SW3 are given in Table 6.1.1.

Run	BSF1	BSF2	BSF3	BSF4	BSF5	BSF6	BSF7
$\overline{Q}$ (m^3/s)	27.8	27.3	29.2	26.9	23.5	27.2	28
Run	BMF1	BMF2	BMF3	BMF4	BMF5	BMF6	BMF7
$\overline{Q}$ (m^3/s)	62.5	60.9	62.4	60.6	59	61	60.7
Run	BWF1	BWF2	BWF3	BWF4	BWF5	BWF6	BWF7
$\overline{Q}$ (m^3/s)	111.1	110.4	110.3	110	108.6	109.9	108.2

6.3 Exchange enhancement by barotropic forcing

We make further comparisons of volume fluxes between the steady run SW3 and the unsteady runs BWF1–BWF7. Note that all these simulation runs have the same friction parameter values (see Tables 4.1.1 and 4.3.3). The volume flux is 89 m^3/s for run SW3, where barotropic forcing is absent. The volume fluxes increase to 108.2 to 111.1 m^3/s for runs BWF1–BWF7, where barotropic forcing is present. This is an exchange

enhancement solely due to the effect of individual barotropic forcing modes. Thus, under the assumption that friction is weak, barotropic forcing can possibly enhance exchange.

A number of investigations (e.g. Armi and Farmer, 1986; Helfrich, 1995) have shown that barotropic forcing can cause volume flux to exceed the theoretical inviscid value or Q_{inv}, which is 125 m^3/s for the Burlington Ship Canal. This does not occur in the Burlington Ship Canal. Although the barotropic forcing is seen to cause volume flux to increase from the steady exchange value, all the time averages of volume fluxes are still below the theoretical inviscid value of $Q_{inv} = 125$ m^3/s. We caution that this result is based on the implementation of individual barotropic forcing modes, not the barotropic forcing as a whole (with all the modes combined).

6.4 The effect of friction

It is difficult to obtain accurate estimates of friction parameters, particularly for interfacial friction between the upper and lower layer that are moving relative to each other. However, once the parameters are determined, the effect of friction on exchange flow is less intricate. An increase of friction simply results in a decrease of volume flux in each layer. For example, as friction increases from weak friction in run SW3, to moderate friction in run SM3 to strong friction in run SS3 (see Table 4.1.1), the volume

flux decreases from 88.68 to 63.76 to 33.78 m^3/s. The results for other steady runs show the same trend.

In fact, the trend that volume flux monotonously decreases with increasing friction holds regardless of the condition of any other model parameters. Runs BWF1, BMF1 and BSF1 (see Tables 4.3.1, 4.3.2 and 4.3.3) show the trend of time average of volume flux (Table 6.2.1) decreasing with increasing friction. One reaches the same conclusion when examining the results for runs BWF7, BMF7 and BSF7 and all other unsteady runs (Table 6.2.1). Thus, regardless of barotropic forcing, the volume flux decreases with increasing friction.

Chapter Seven: Conclusions

A two-layer internal hydraulics model has been established for simulating exchange flow through a straight, rectangular channel like the Burlington Ship Canal. We present the procedures for determining model parameters pertinent to a given channel's geometry, friction and time-dependent barotropic forcing. For the case of the summer exchange through the Burlington Ship Canal, we determine the model parameters using field measurements, and successfully verify the model through thorough sensitivity test and comparisons with laboratory channel experiments of exchange flow. The two-layer internal hydraulics model can be easily adapted to other exchange flows.

Direct comparisons of interface height and volume flux between model predictions and the laboratory experiments are made. The comparisons are excellent. The predicted interface profiles are plotted though the middle of the experimental data and the predicted volume fluxes are within 10% of the laboratory measurements. These comparisons indicate that sidewall friction is important to accurate determination of volume flux. This is to the contrary of early judgment.

Our steady exchange simulations confirm that the exchange flow through the Burlington Ship Canal is highly frictional. The volume flux of the frictional exchange through the canal is about one half the theoretical inviscid flow rate of 125 m^3/s. It is also

shown that the exchange can be described reasonably well by a two-layer hydraulics model.

Our simulations of unsteady exchange flow for the Burlington Ship Canal have captured the observed fluctuations of interface heights and layered velocities, as observed in the field. We demonstrate that individual barotropic forcing modes cause the flow in the upper and lower layer to oscillate in time. The forcing modes can cause the flowing layers to reverse their directions and can arrest the flowing layers during certain phases of the forcing cycle. In terms of time averages of volume fluxes, the individual barotropic forcing modes do not have significant impacts. Therefore, for practical purposes, steady exchange flow theory may be adequate to describe the exchange flow through the Burlington Ship canal.

Given the uncertainties in estimates of friction, we consider the scenarios of strong and weak friction. There are volume flux reductions with increasing frictional effects. This is regardless of barotropic forcing. If friction is weak, strong barotropic forcing modes appear to enhance the exchange through the canal. If friction is strong, the forcing modes are seen to inhibit the exchange. These results are based on the implementation of individual barotropic forcing modes. No further conclusion can be made about the effects of the time-dependent barotropic forcing as a whole.

This study represents an extension to earlier investigations of exchange flow. We incorporate both friction and barotropic forcing of multiple frequencies, although implemented individually. This study has ignored fluid mixing and recirculation, which would be interesting to consider in future studies.

Chapter Eight: Suggestions and Recommendations

Future studies of exchange flow ought incorporate barotropic forcing as a whole with all significant modes combined, as opposed to imposing individual modes in this and other existing studies. For barotropic oscillations triggered by the winds blowing over a reservoir (e.g. Lake Ontario), although individual modes of the oscillations have their frequencies more or less regulated by the reservoir's geometric characteristics, the combination of the modes may be random. The simple reason is that the modes can have different initial phases that are unrelated to each other. A stochastic approach would be appropriate to incorporate barotropic forcing of multiple frequencies.

This study highlights the importance of friction to the determination of volume flux in exchange flow. An improvement in evaluation of friction parameters, in particular the interfacial friction factor, needs to be made. Given that interfacial friction is associated with fluids that are moving relative to each other, an improved understanding of the dynamics of stratified shear flows would be required to obtain accurate estimates of interfacial friction.

Water-quality studies for Hamilton Harbour may use the results from this hydraulic study. The harbour holds approximately 280 million m^3 of water. The predicted volume fluxes are in the range of $Q_{pred} = 34-89\,m^3/s$. Over the time period of one month in the

summer, the total flux due to the exchange flow amounts to about 30% of the harbour volume if the lower limit is considered, and about 80% of the harbour volume if the upper limit is conisdered.

The signficance of the volume flux due to the exchange flow becomes clear when compared to natural streams and waste effluents that enter the harbour. Accordingt to Hamblin (1989), natural streams that enter the harbour bring 127 million $m^3$of water per year, and the amount of municipal and industrial effluent that enters the water is a staggering 102 million m^3 per year. Constituents of this effluent are dangerous fertilizers, pesticides and herbicides. Many of these contain very hazardous metallic, organic and bacterial contaminants. During the periods of the exchange flow, large amounts of water are exchanged between the harbour and the lake. Thus, it is important to incorporate the water exchnage due to the exchange flow when determining the water quality of either body.

References

Armi, L. (1986). "The hydraulics of two flowing layers with different densities." *Journal of Fluid Mechanics*, 163: 27–58.

Armi, L., and Farmer, D. (1986). "Maximal two-layer exchange flow through a contraction with barotropic net flow." *Journal of Fluid Mechanics,* 164, 27–51.

Armi, L., and Farmer, D. (1988). 'The flow of Mediterranean Water through the Strait of Gibraltar.' *Progress in Oceanography,*21, 1–105. doi:10.1016/0079-6611(88)90055-9.

Assaf, G., and Hecht, A. (1974). "Sea strait: a dynamic model." *Deep-Sea Research*, 21, 947-958.

Barica, J.,Poulton, D.J.,Kohli, B.,& Charlton, M.N. (1988). 'Water exchange between Lake Ontario and Hamilton Harbour : Water Quality". *Water pollution Research Journal of Canad,* 23(2):213-236.

Barica, J. (1989). "Unique limnological phenomena affecting water quality of Hamilton Harbour, Lake Ontario." *Journal of Great Lakes Research,* 15(3): 519-530.

Chaudhry , M. Hanif (2008). "Open-channel flow"*New York, NY, Springer*, 2nd edition

Chow, V. T. (1959). "Open channel hydraulics." *McGRAW-Hill, Book Company.*

Dick, T. M. and Marsalek, J.(1973). "Exchange flow between Lake Ontario and Hamilton Harbour." *Environment Canada Inland Waters Directorate*, 1973; Scientifc Series No. 36.

Farmer, D. & Armi, L. (1986)."Maximal two-layer exchange over a sill and through the combination of a sill and contraction with barotropic flow". *Journal of Fluid Mechanic,* 164, 53–76.

Fox, M. E., Khan, R. M. and Thiessen, P. A.(1996). "Loading of PCBs and PAHs from Hamilton Harbour to Lake Ontario." *Water Quality Research Journal of Canada*, 31(3): 593–608.

Gorrie, P.(1987). "Cleaning up Hamilton Harbour." *Canadian Geographic*, 107: 34–35.

Greco, S. L. (1998). "Two-layer exchange flow through the Burlington Ship Canal." *M.A.Sc. thesis, Department of Civil Engineering, the University of British Columbia,* 114 pp.

Gregg, M. & Ozsoy, E. (2002)."Flow, water mass changes, and hydraulics in the Bosphorus." *Journal of Geophysical Research*, 107, 1–2. 10.1029/2000JC000485.

Gu, L. (2001). "Frictional exchange flow through a wide channel with application to the Burlington Ship Canal." *PhD thesis, University of British Columbia.*

Gu, L. and Lawrence, G. A.(2005). "Analytical solution for maximal frictional two-layer exchange flow." *Journal of Fluid Mechanics*, 543: 1–17.

Hamblin, P.F., He, C. (2003). "Numerical models of the exchange flows between Hamilton Harbour and Lake Ontario" *Journal of Civil Engineering*, 30: 168–180

Hamblin, P. F.(1982). "On the free surface oscilaations of Lake Ontarion." *Limnology and Oceanography*, 27(6): 1039–1049.

Hamblin, P. F. and Lawrence, G. A.(1990). "Exchange flows between Hamilton Harbour and Lake Ontario." *Proceedings of the 1st Biennial Environemntal Speciality Conference, CSCE*, 1: 140–148.

Hamblin, P. F.,and Murthy, T. S. (1974). "Helmholz resonance in harbours of great lakes." *Proceedings of the 17th Conferance Great Lakes Research*, 399-411.

Hansen,W. (1962). "Tides." *In. Hill, M.N., Goldberg, E.D., Iselin C. O'D. and Munk, W.H. (editors), The Sea. John Wiley & Sons Freeman, N. G.*, pp. 764-801

Helfrich, K. R. (1995). "Time-dependent two-layer hydraulic exchange flows." *Journal of Physical Oceanography,* 25: 359–373.

Hogg, A., Ivey, G.N., and Winters, K.B. (2001). "Hydraulics and mixing in controlled exchange flows." *Journal of Geophysical Research,* 106: 959 – 971.

Hutchinson, G.E. (1957). "Treatise on Limnology." *John Wiley & Sons*, pp. 333.

Jarosz, E.,Murray, S. P. & Inoue,M. (2005). "Observations on the characteristics of tides in the Babel Mandab Strait." *Journal of Geophysical Research,* 110, C03015. doi:10.1029/2004JC002299.

Kohli, B.(1979). "Mass exchange between Hamilton Harbour and lake Ontario." *Journal of Great Lakes Research*, 5(1): 36–44.

Lawrence, G.A. (1990). "On the hydraulics of Boussenesq and non-Boussinesq two-layer flows." *Journal of Fluid Mechanics,* 215: 457 – 48.

Lawrence, G., Pieters, R., Zaremba, L., Tedford, T., Gu, L., Greco, S. and Hamblin, P. (2004). "Summer exchange between Hamilton Harbour and Lake Ontario." *Deep-Sea Research,* 51, 475–487.

Li, S. S. and Lawrence, G. A.(2009). "Unsteady two-layer hydraulic exchange flows with friction." *Journal of Fluid Mechanics*, 633: 99–114.

Ling, H., Diamond, M. and MacKay, D.(1993). "Applicairon of the QWASI Fugacity/Aquivalence model to assessing sources and fate of contamiants in Hamilton Harbour."*Journal of Great Lakes Research*, 19(3): 582–602.

Millero, Frank J.(2000). "The Equation of state of lakes." *Aquatic Geochemistry*, Vol.6,p.1-17.

M.O.E. (Ontario Ministry o f the Environment).(1989). "Stage 1 Report: Environmental conditions and problem definitions." *Remedial Action Plan for Hamilton Harbour.*

M.O.E. (Ontario Ministry o f the Environment).(1992). "Stage 2 A Report: Goals, options and recommendations." *Remedial Action Plan for Hamilton Harbour.*

Henderson, F.M. (1966). "Open channel flow." *MacMillan.*

Morozov, E. G., Trulsen, K., Velarde, M. G. & Vlasenko, V. I. (2002). "Internal tides in the Strait of Gibraltar." *Journals of physical Oceanogrraphy*, 32, 3193–3206.

Ottensen-Hansen, N. & Moller, J. (1990). " Zero blocking solution for the Great Belt Link." *In The Physical Oceanography of Sea Straits (ed. L. Pratt),* pp. 153–170. Kluwer.

Palmer, M.D., & Poulton, D.J. (1976). "Hamilton Harbour: Periodicities o f the physiochemical process." *Limnol. Oceanog*, 21:118-127.

Rao, D.B. and Schwab, D.J. (1976). "Two dimensional normal modes in enclosed basins on a rotating Earth: application to Lake Ontario and Superior." *Transactions of the Royal Society of London, A.* 281:63-96

Schijf, J. B. & Schonfeld, J. C. (1953). "Theoretical considerations on the motion of salt and fresh water." *Proceedings of the Minnesota International Hydraulics Convention,* 321-333.

Tedford, E. W.(1998). "Exchange flow through the Burlington Ship Canal." *M.A.Sc. thesis, Department of Civil Engineering, the University of British Columbia*, 63 pp.

Wu, J., Tsanis, I. K. and Chiocchio, F.(1996). "Observed currents and water levels in Hamilton Harbour." *Jounral of Great Lakes Research*, 22(2): 224–240.

Zaremba, L. J., Lawrence, G. A. & Pieters, R. (2003). "Frictional two-layer exchange flow." *Journal of Fluid Mechanics,* 474, 339–354.

Zhu, D. Z. and Lawrence, G. A. (2000). "Hydraulics of exchange flows." *Journal of Hydraulic Engineering, ASCE,* 126: 921–928

Appendix A: Conceptual Model (Flow Chart)